* CREST *

Second Specialist Meeting on

Sodium-Fuel Interaction in Fast Reactors

Ispra, 21st-23rd November 1973

Progress Report on the Molten UO_2 Drop Experiment

H. MIZUTA, F. HIRABAYASHI,

N. YOKOZAWA, Y. FUKUSHIMA

Power Reactor and Nuclear Fuel Development Corporation

Tokai, Ibaraki, Japan, 319-11

ABSTRACT

A series of 30 experiments were performed to examine the fragmentation characteristics of Sodium-Fuel Interaction by dropping molten UO_2 into sodium. In this experiment, annular UO_2 pellets were heated by the center line heating of tungsten rod, and the molten UO_2 droplets fell into the sodium tank. The fragmentations of the droplets on the surface of liquid sodium were photographed with high speed camera at 500~2000 pictures/sec. The pressure and temperature of sodium tank were measured.

The particle characteristics of the UO_2 residue was examined on the particle size distribution, the particle surface condition, and the grain characteristic of the particles for the fragmentation mechanism. These examination indicates that the UO_2 particles can be assumed to be spherical and to have the log-normal distribution function.

The most pessimistic particle size distribution at present can be represented by the equation

$$f_i(D) = 2.317 \exp\left(\frac{-(\log D - 2.267)^2}{0.9442}\right)$$

where $f_i(D)dD$ = weight percent of particles in size range D to D + dD.

1. INTRODUCTION

The objective of PNC Fuel-Sodium Interaction Project is to develop the mathematical models for pin failure, subassembly failure and core meltdown with the execution of the out-of pile tests on the possible pressure and its ratio to the total mechanical energy from sodium-fuel interaction. During the current reporting period, the major out-of-pile work has been done on the molten UO_2 drop test. The device and method of this test were presented in the last SFI Specialist Meeting in Grenoble. So in this paper, the description on the test is made very briefly.

The schematic diagram of this test is shown in Fig. 1. Annular UO_2 pellet was heated up to about 3020°C and the molten UO_2 droplets fell into the sodium tank. The sodium tank was instrumented with a pressure gauge at the bottom and a thermocouple near the center of the tank. The temperature of the droplet was monitored with the optical pyrometer. The number of the fallen droplets and their fragmentation behavior were taken with the high speed camera.

2. EXPERIMENTAL RESULTS

Summary of the 12 runs out of 30 runs is listed in Table 1. Although the temperature measurement of the droplet was very difficult, it is the most important factor for the fragmentation. So the temperature was evaluated as the following way.

The average temperature of the melted area of the pellet is estimated about 3020 C° with the electric heating data.

When a droplet left the stopper of the heating device, the droplet temperature was at least above the melting point which was confirmed with the optical pyrometer. Finally the temperature of the droplet just before entering the sodium is estimated 2840 °C at the center and 2200~2500 °C at the surface with the transient heat transfer calculation (for example, the droplet dia. = 2.6 mm, time interval to hit the sodium surface = 0.288 sec.).

The observation of the droplet behaviors was summarized in Table 2. The high speed movie gave the droplet numbers, the droplets entering condition and the sodium vaporization delay time. Two movie pictures of the detailed sequence of events during the entering and fragmentation of UO_2 in sodium are shown in Fig. 2 and 3. Sometimes the sodium explode or was pressurized (Fig. 2) and sometimes it did not (Fig. 3) when the sodium was pressurized, the droplet was completely submerged in the sodium. And after the sodium explode, the fragmented and solidified UO_2 droplets were ejected as shown in Fig. 2. The splashed sodium and ejected UO_2 droplets were examined after the event as shown in Fig. 4. Those sodium and UO_2 were collected carefully and weighed.

The temperature hystories in the sodium tank are shown in Fig. 5~Fig. 8. These temperature hystories indicate that the sodium temperature was raised quite abruptly and down slowly. But this data are of little direct value for quantitative temperature analysis due to the lack of the relative distance between droplet entering position and the thermocouple position, and to relatively large time constant of thermocouple

(2 sec). So the temperature measurement in the sodium needs inprovement.

The typical pressure pulse in sodium at the time of the UO_2 droplet contact, is shown in Fig. 9. The duration time of the pulse was read about 1 msec. The minumum response frequency of the pressure transducer was 40 KHZ. Therefore, the value of the pressure pulse was valid. Fig. 10 and Fig. 11 show the total pressure hystories for Run 20 and Run 23 respectively. The number in the chart indicates the sodium pressurization times. Comparing this pressurization number with the droplet entering number of the high speed movie, the sodium pressurization did not occur everytime at the droplet entering. The condition of this pressurization seemed to be sensitive to the droplet surface temperature.

The careful examination of the total pressure hystory for each run lead that the duration time seemed to be come longer as the droplet number increased. That trend is listed in Table 3.

The relation between the pressure peak in the sodium and the UO_2 particle size is shown Table 4 and Fig. 12. It can be said that the peak pressure increases as the particle size becomes finer.

3. PARTICLE SIZE DISTRIBUTION

Fig. 13 shows the collected UO_2 residue of 15th run as the typical sample. Almost all of the shell type particles yielded from the large spherical particle during collecting

the residues. The large particle was very collapsible due to the numerous cracks in it. The sodium in the particle as shown in Fig. 14, was considered to get into the inside of the particle through those cracks after the particle had been solidified.

UO_2 particles for each run were screened to determine the particle size distribution. As the particles were very collapsible, the screens which were the hand-shaker type standard sieve series of the 8, 20, 65 mesh sizes, were sieved very softly. Fig. 15 shows the separated UO_2 particles for Run 28. The particles size below 210 μ is the most important factor for the heat transfer from UO_2 to sodium. Therefore, the average particle size in this range was re-evaluated with SEM (Scanning Electron Microscope) photographic techniques and the section area measurement method. The particle distributions for each run are listed in Table 5. Fig. 16 shows the UO_2 particle distribution assuming that the distribution can be represented by Rosim-Rammler distribution. The arithmetic average was used for the representative value of a range except + 8 mesh and -65 mesh in which the average particle size was measured directly. The particle distribution is not the exact log-normal distribution, but the data of the particle size can be arranged with the log-normal distribution.

4. PARTICLE CHARACTERISTICS

For getting the information on the UO_2 droplet fragmentation, the particle characteristics was investigated on the particle shape, particle surface (the specific surface), grain size, grain growth type, void distribution and cracks with microscope, SEM, ceramography and BET method.

4.1 Large particle (1~3 mmφ)

The larger size particles were regular in shape of sphere and liquid droplet as shown in Fig. 15, and of cylinder in Fig. 17. The shape of the droplets in considered to be determined by the UO_2 viscosity just before entering into the sodium; the higher viscosity (the lower UO_2 temperature) seemed to make the cylindrical shape of the droplets.

There were two types of the grain size of UO_2 in this range. The larger particle (~3 mmφ) appeared to have the larger grain and cracks which run from the centeral void to the surface as shown in Fig. 18. The smaller particle (~1 mmφ) appeared to have the smaller grain and cracks as shown in Fig. 19.

4.2 Small particle (<210 μ)

Fig. 20 shows the smaller particles shape under 65 mesh. They were more irregular in shape than the larger one, with being relatively spherical, ellipsoidal, flat as shown in Fig. 21~23. The surface condition of the particles was mostly smooth. The rough surface in the figures seemed to be collapsed during collecting and sieving the particle.

Fig. 23 and 24 show that the particle with a hole. This type of the particle was often seen in other run. The mechanism of the hole formation was not clear.

Fig. 25 and 26 show the typical shapes of the small particles (~40 μ), which had the smooth surface and cracks.

The particle in Fig. 25 seemed to be expanded on the surface due to the inside pressure.

Fig. 27 shows the spherical particle with many, regular

cracks. So it is easy to understand that the particle is very collapsible.

Two particles fused together as shown in Fig. 28. The particle of this type was also often seen.

The microstructure of the small particle was consisted of columnar grain growth to the surface and very fine equi-axial grain growth at the center or near the central void as shown in Fig. 29~Fig. 32. This central void was considered to form due to the solidification of the particle from the surface (~10% density increase).

Fig. 33 shows that one solidified particle was covered with other particle. The Close-ups of Fig. 33 (Fig. 34 ~ Fig. 36) indicated the solidification characteristics.

The specific surface of under 65 mesh particles for Run 27, was measured 0.32 m^2/g with the BET[1)] method. This value corresponds that the average particle diameter is 1.70 μ. Comparing this diameter with the 52 μ diameter measured with the section area method, the BET diameter is the one 31st of the section area diameter. This means that the cracks of the particle divide the particle into one 31st.

---

1) BET method (Brunauer, Emmett and Teller)

In this method, a stream of gas is passed over a cooled UO_2 sample, and the surface area of the sample is determined by measuring the amount of absorbed gas. The gas stream consists of a known mixture of a suitable adsorbate (nitrogen) and an inert gas carrier (helium).

The observations on the UO_2 particle characteristics are summarized as follows;

1. The larger particles ($\sim$1 mmϕ) were smooth on the surface and spherical in shape. There were two type of the microstructure, that is, the larger grain (amorphous), and the smaller regular grain. The crack was mainly transgrannular, where the fracture seemed to occur well below the brittle-to-ductile transition temperature ($\sim 1600^{\circ}C$).

2. The smaller particles ($\sim 40\ \mu\phi$) were also smooth surface with a high percentage of the spherical and the ellipsoidal which freezed without further fragmentation. Particles with the irregular particles yielded from the larger particles at the fragmentation. The equi-axial grain growth occurred near the center of the particle. On the other hand, the columnar grain growth occurred at the surface ot it. Almost all of the cracks were integranular, where the fracture seemed to occur at or just above the transition temperature.[1)]

3. Both particles had the extensive cracks, thus, they were very collapsible.

5. DISCUSSION OF THE FRAGMENTATION

The modelson the fragmentation of hot molten materials as they are mixed with the cold fluid, have been presented as follows;

1. Liquid entrapment model;[2)] as the water is trapped between the molten aluminum and the container, it evaporates rapidly and causes the fragmentation of the aluminum.

2. Impact model;[3)] as a water column strikes the molten

aluminum, the violent disruption and dispersion of the molten aluminum occurs.

3. Hydrodynamic (Critical Weber Number) model;[4] as the inertial (hydrodynamic) forces exerted on the low melting metals (Pb, Sn, Bi, Hg) by the room temperature water, overcome the surface tension of the globule, the fragmentation occurs' (the higher the Weber number, the greater the fragmentation).

4. Liquid entrainment model;[5] as the water is trapped by the molten metal (Al, Pb), rapid vaporization of the molten metal into the water.

5. Two-fluid nozzles model;[6] as the entire energy imparted to the molten fuel is assumed to come from the flowing sodium vapor, the relationship for two-fluid nozzles can be used.

6. Turbulent mixing model;[7] as the jet of molten materials strikes the cold fluid, the turbulent mixing occurs and it increases the specific surface area between molten materials and cold fluid.

7. Homogeneous nucleation model;[8] as Freon-11 (normal boiling point 23.8°C) are injected into hot water (70~90°C), the liquid jet breaks up according to Weber Number (entrainment-wetting-superheat mechanism).

8. Free-contact (Violent boiling) model; as a molten metals (V, Ti, Zr, Stainless Steel, U, etc.) cools through the sodium temperature which is well above the sodium boiling temperature,

(a) the violent growth and collapse of sodium vapor bubbles break up the molten metals,[9]

(b) the collapse of a vapor film around the molten metal yield the thermal shock in the solidified metals. This thermal shock may cause the fragmentation,[10]

(c) the melting of the hot material should be less than the minimum temperature required to sustain stable film boiling after the surface of the molten material (necessary condition).[11]

9. Shell model; as the molten material is suddenly cooled at the surface, both the steep temperature gradient and the solidification occur on the surface, they cause the large tangential thermal stress at the solidified surface and the pressurization of the liquid inside the molten materials. Those pressure stress and thermal stress cause the fragmentation.[12,13]

These models can be categorized as the interaction of a) liquid (molten material)-vapor (cold fluid), b) liquid-liquid, c) solid-liquid with the surface temperature of molten material. If these models are applied to molten UO_2-sodium interaction, it can be plotted as shown in Fig. 37.

The most appropriate model to describe the fragmentation behavior of our experiment is believed the shell model shown in Fig. 38.

As a droplet with the solidified surface drops into the sodium, the surface temperature is cooled below the brittle-to-ductile temperature and the solidification causes the pressurization inside the droplet. If the total tangential stress in the elastic region exceeds the fracture stress, the fractures occur. At the time of fracture, if the pressure of the inside is high, the extensive fragmentation would occur. Because of

the difficulty of the surface temperature estimation, the calculation of fragmentation is not completed yet.

The particle distribution of UO_2 after the fragmentation is the complex function of fuel temperature, sodium temperature, fuel mass, coolant mass, fission ga, inert gas, surface tension of fuel, fuel cooling rate, subcool of sodium, O/M ratio of fuel, fuel composition, burnup of fuel, mixing velocity and mixing geometry in the molten fuel and sodium interaction zone. The available data of the particle distribution in the UO_2-sodium and UO_2-water system at present, are TREAT[14] S-series in-pile data, Armstrong[15] out-of-pile data and SPERT[16)17)18)] CDC-series in-pile data. Fig. 39 is a plot of these particle size distributions.

Any decisive parameter which determines the particle size distribution, can not be found in these data. Even the coolant difference comparing TREAT data with SPERT data, does not cause the large difference of the particle size distribution. The most pessimistic distribution function of the fuel particle is obtained from Fig. 39 with considering the maximum slope and minimum mean value assumming the log-normal distribution. That function is $f_i(D) = 2.317 \exp\left(\frac{-(\log D-2.267)^2}{0.9442}\right)$, where D = the particle diameter in micrometer. The particle size distribution is not exact log-normal distribution. But if the log-normal distribution is used for the SFI analysis, it is conservative because the larger particle is underestimated.

6. CONCLUSION

1. A droplet with the solidified surface have the possibility of the extensive fragmentation. This solid-liquid fragmentation is the base of the particle size distribution because all the droplet is cooled to the sodium temperature.

2. For the SFI safety analysis, the assumption of (a) the spherical UO_2 particle and (b) the log-normal distribution function is conservative and reasonable.

3. The particle characteristic study of UO_2 is revealed very useful for the development of the fragmentation mechanism.

The future SFI out-of-pile experimental programs in PNC, are;

1. Sold UO_2 fragmentation study with the transient heat transfer apparatus.

2. Fuel pin melting study in the several fuel pins.

Table 1 Summary of the Molten UO_2 Data

Run Number	Na Initial Temp. ^{o}C	Na Initial Volume cm^3	Quantity of Melt Droplets g	Peak Pressure Kg/cm^2
1	200	170	Failed to collect the residue	Failed to measure
9	230	170	"	2.73
15	300	120	10.20	0.1
20	300	120	14.75	1.2
21	200	120	14.85	1.42
22	200	104	11.60	1.05
23	300	123	12.78	3.50
24	200	99	Failed to collect the residue	1.65
25	200	187	18.51	Failed to measure
26	200	32	7.87	1.3
27	200	52	9.99	0.1
28	200	52	1.50	0.1

Table 2 Summary of the Molten UO_2 Drop Test Observation

Run Number	Droplet Number		Droplet Entering Condition	Pressurization	Sodium Vaporigation Delay time, msec	Na Splash
	High Speed Camera	Pressure Record				
1			Large spherical droplet	failed to measure	2	Not observed
9	6		Large spherical droplets	No	a	Yes
15	1 4		Small droplet	Yes	a	No
20	7	6	Small Droplet	Yes	5	Yes
21	16	8	Droplets fell almost simultaneously	Yes	a	Yes
22	7	3	Droplets fell like a string(cylinder shape)	Yes	3.6	No
23	11	9	"	Yes	7	Yes (26%)
24	10 16		"	Yes	a	Yes (25%)
25	18		"	Yes	a	Yes (37%)
26	4		Large spherical droplet	Yes	a	Yes
27	1		"	Yes	1.5	Yes
28	1		No film record	Yes		No

a : The ejection of UO_2 particle was not observed.

Table 3 Duration Time of the Sodium Pressure Pulse

Run	Droplet Number	Duration Time (m.sec)	Run	Droplet Number	Duration Time (m.sec)
20 Na Temp. 300°C	1	0.8	21 Na Temp. 200°C	1	0.9
	2	0.9		2	1.0
	3	1.0		3	0.9
	4	1.4		4	1.3
	5	1.9		5	1.8
	6	1.8		6	1.8
	7	2.0		7	2.1

Table 4 The Correlation between Max. Pressure Peak and Particle Size

Run Number	Max. Pressure Peak Kg/cm^2	Particle Size -65 Mesh (W/o)
15	0.1	0.13
20	1.2	13.6
21	1.42	18.1
22	1.05	0.39
23	3.5	19.47
26	1.3	7.2
27	0.1	6.4

Table 5 UO_2 Particle Distribution

Particle Range / Run No.	< 210 μ		210 μ ~ 840 μ		840 μ ~ 2380 μ		> 2380	
	Average Particle Dia.	w/o	Average Particle Dia.	w/o	Average Particle Dia.	w/o	Average Particle Dia.	w/o
15	41	2.2%	525	3.8%	1610	38.2%	5100	27.8%
20	50	22.1	"	27.7	"	31.2	5740	16.2
21	53	18	"	26	"	41.5	3020	10.1
22	48	1.2	"	11.8	"	21.7	4250	56.8
23	43	20	"	27.8	"	36.0	5440	10.7
24	51	26.8	"	44.2	"	27.9	2100	0.9
25	52	15.2	"	15.5	"	41.8	5300	22.3
26	60	7.2	"	18.0	"	27.8	4300	30
27	52	5.0	"	14.4	"	19.6	5100	45

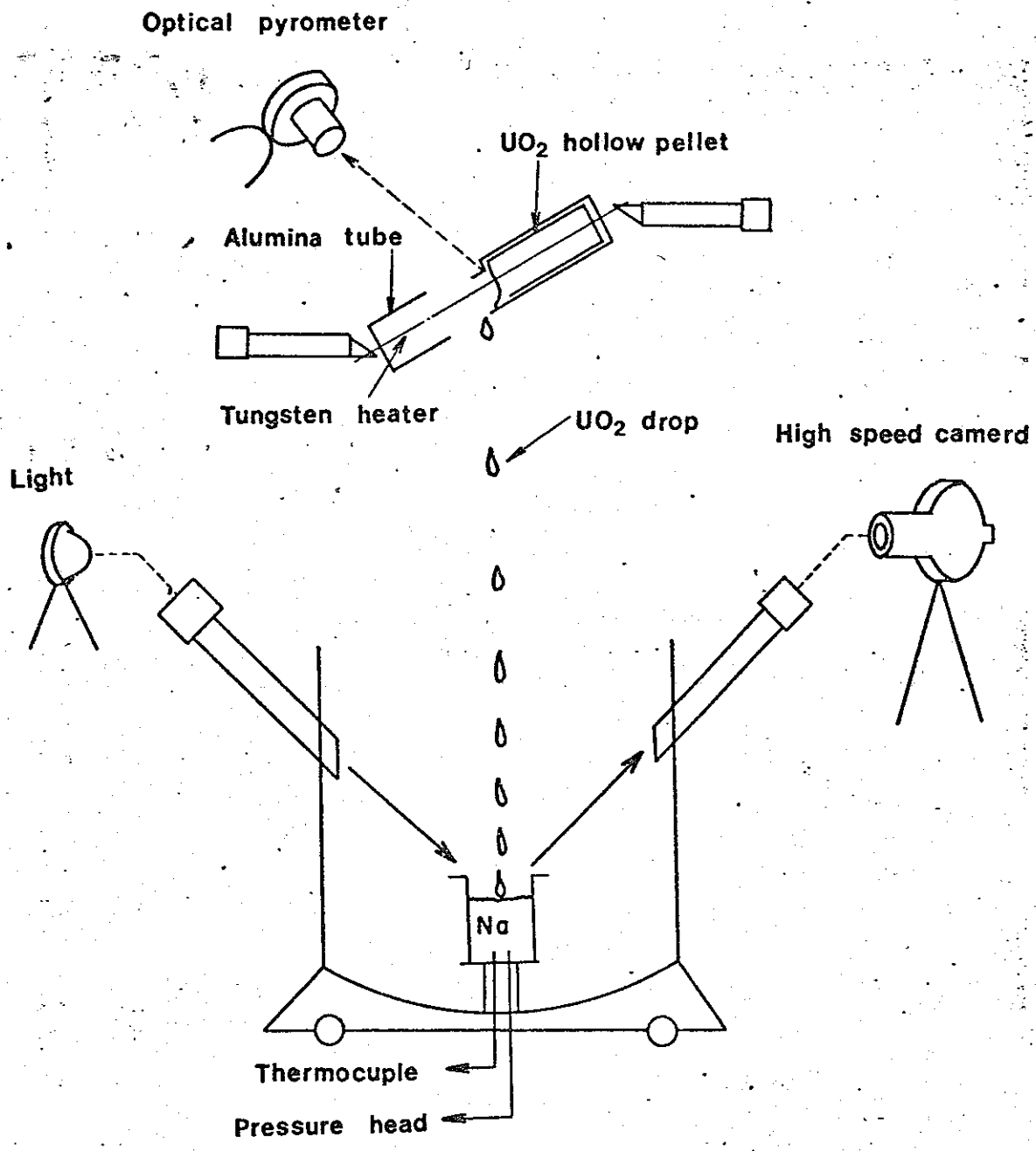

Fig. 1 Schematic diagram of the molten UO_2 fragmentation experiment.

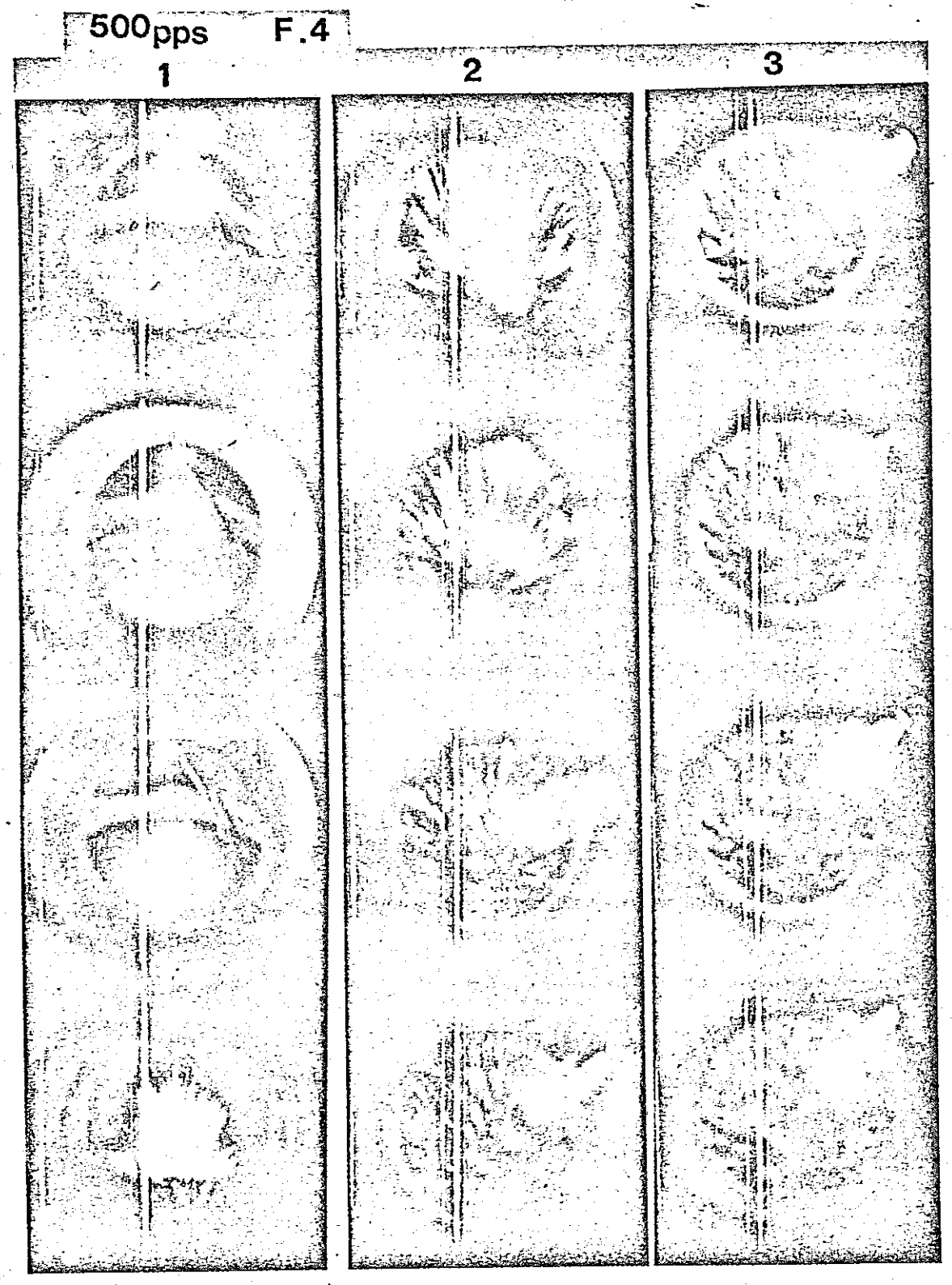

Fig. 2 High speed movie for Run 1.

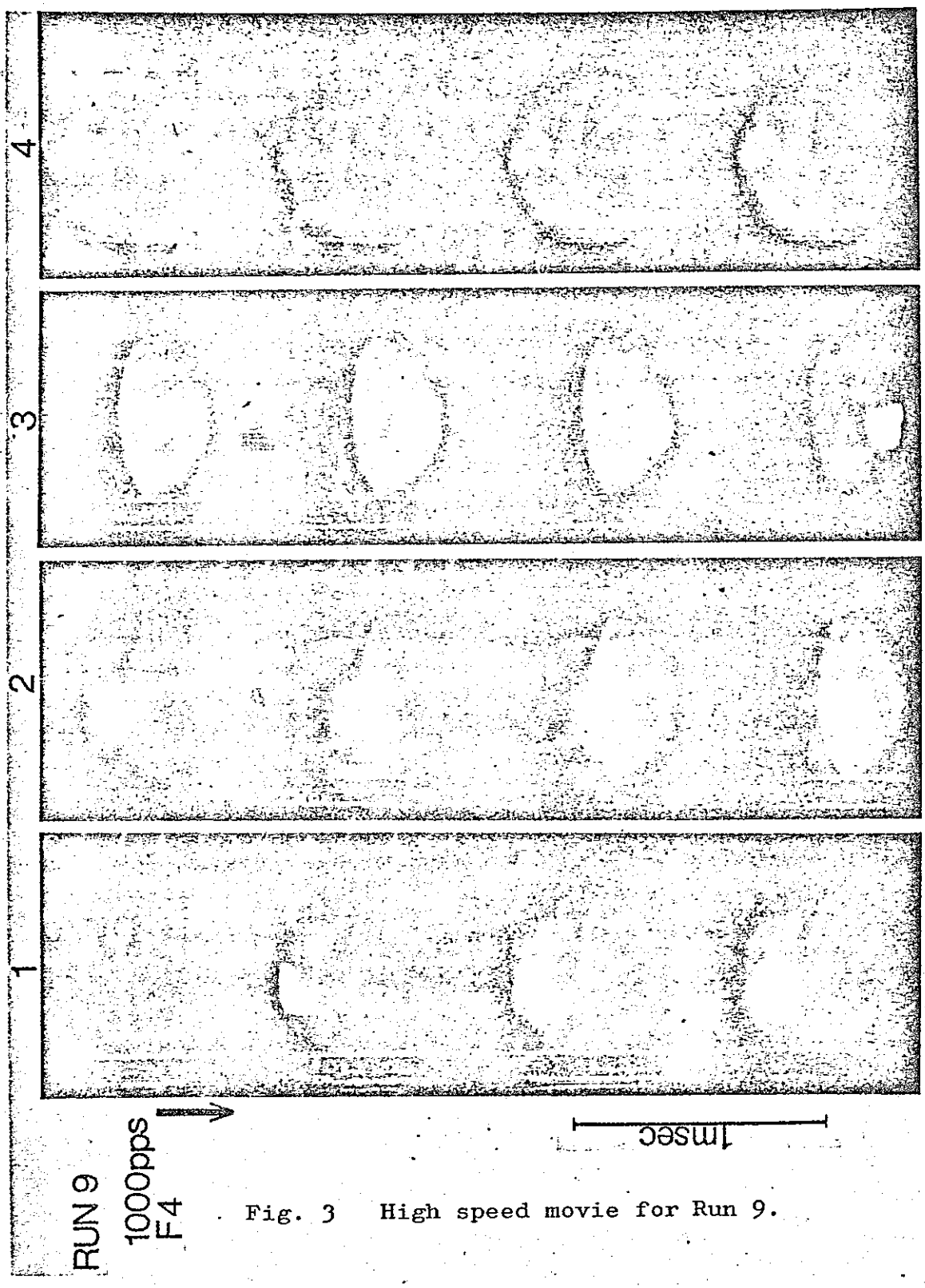

Fig. 3 High speed movie for Run 9.

Fig. 4 Ejected sodium and UO_2 droplet.

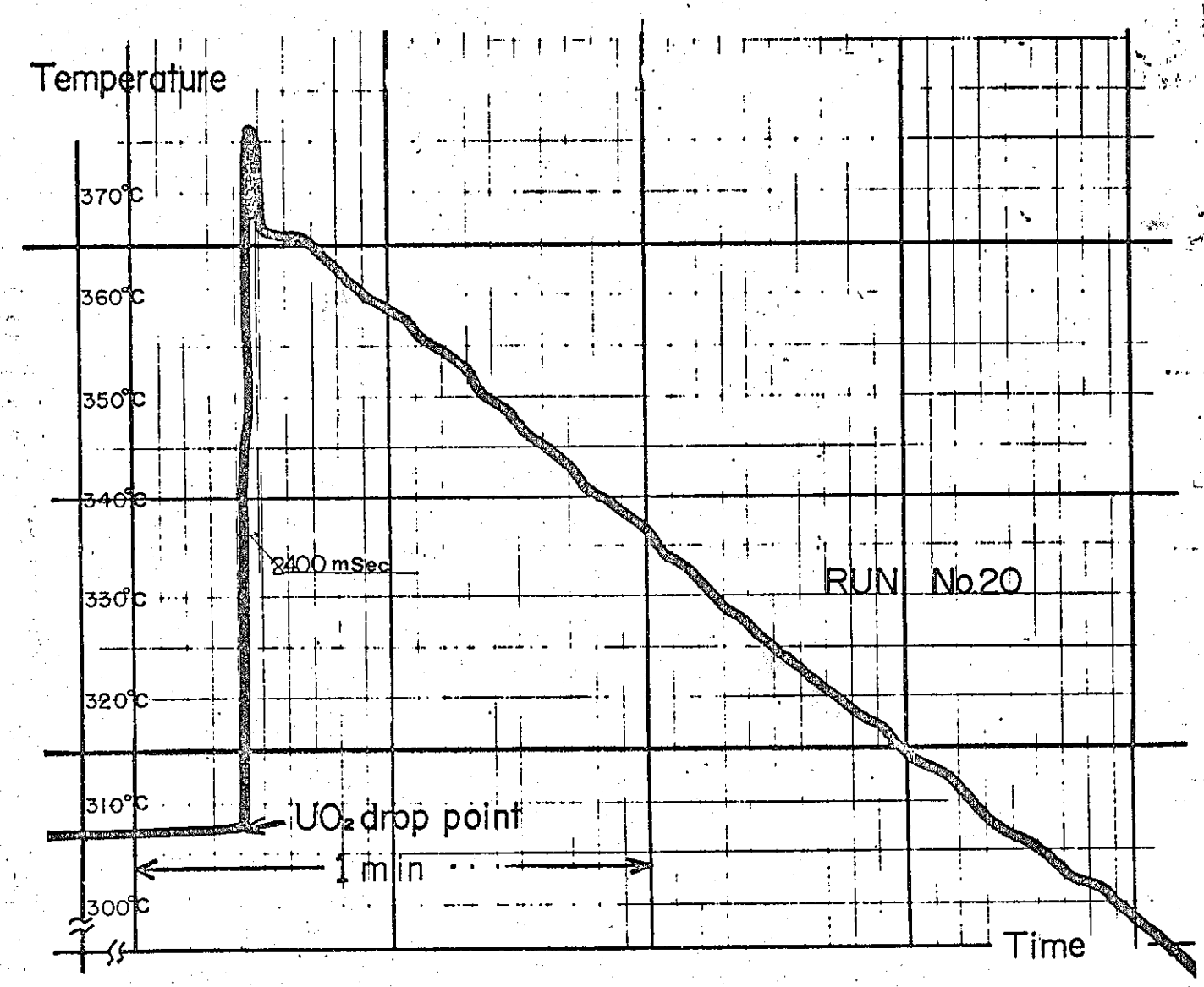

Fig. 5 Sodium temperature distribution.

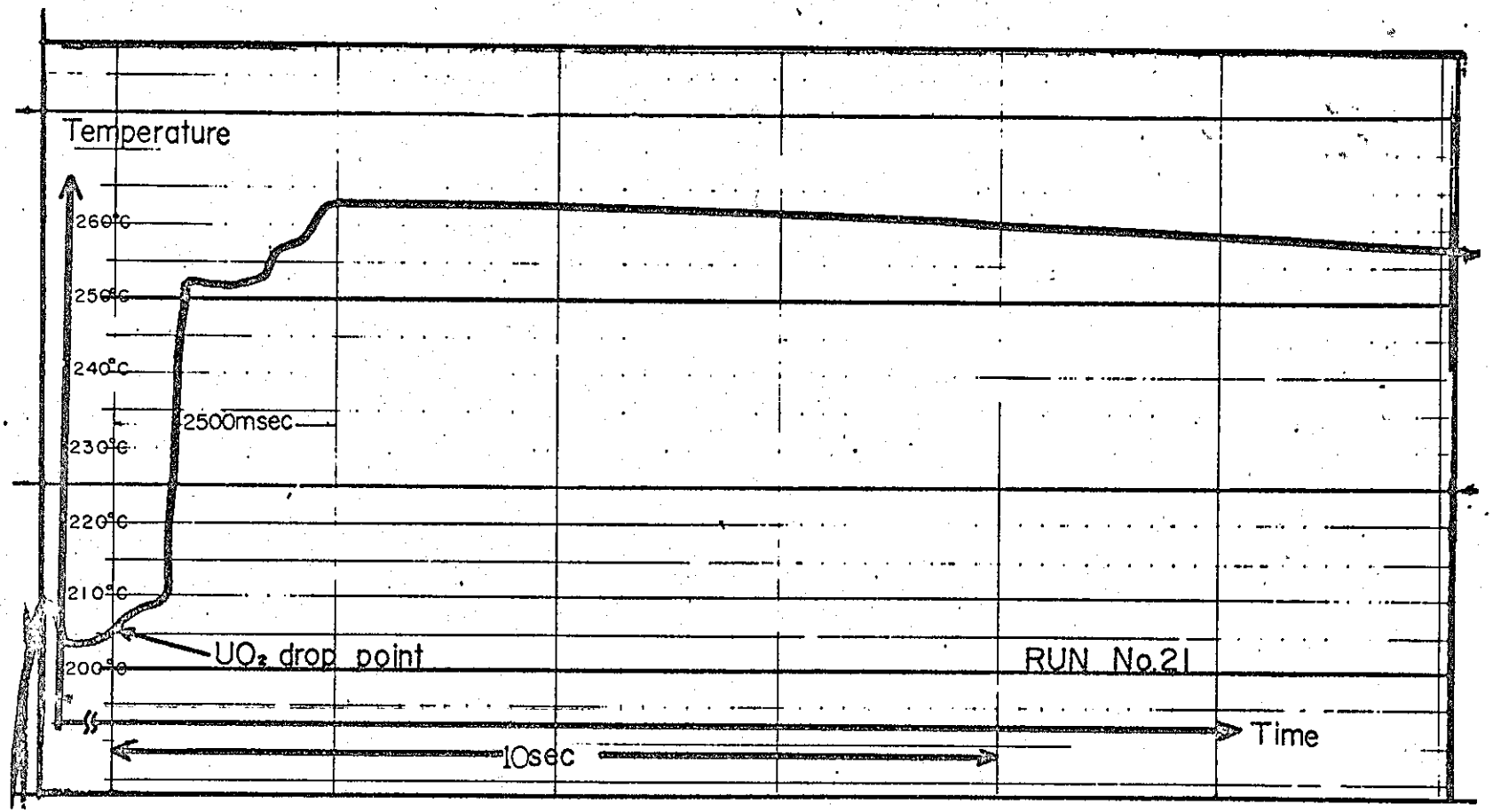

Fig. 6 Sodium temperature distribution.

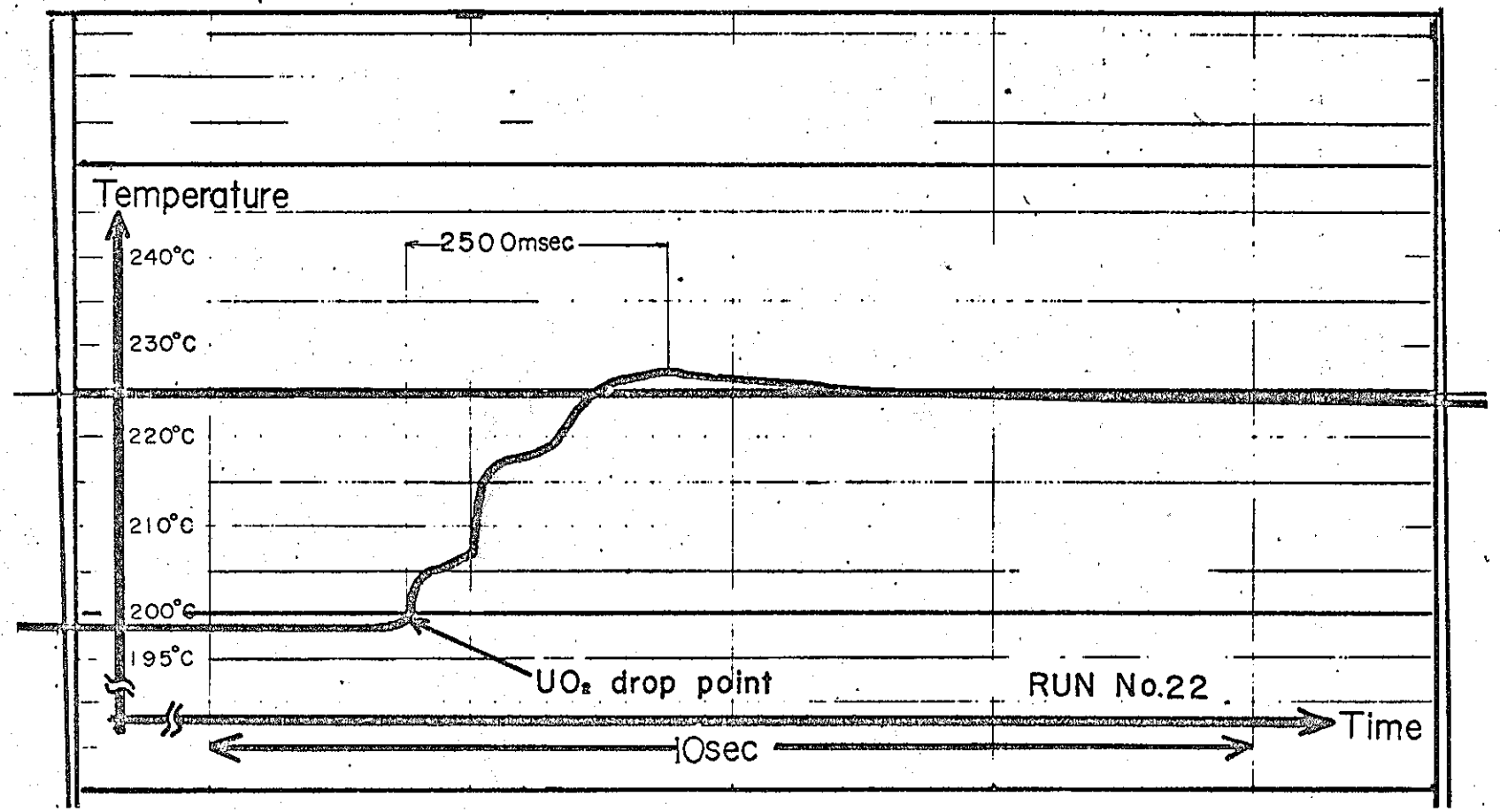

Fig. 7 Sodium temperature distribution.

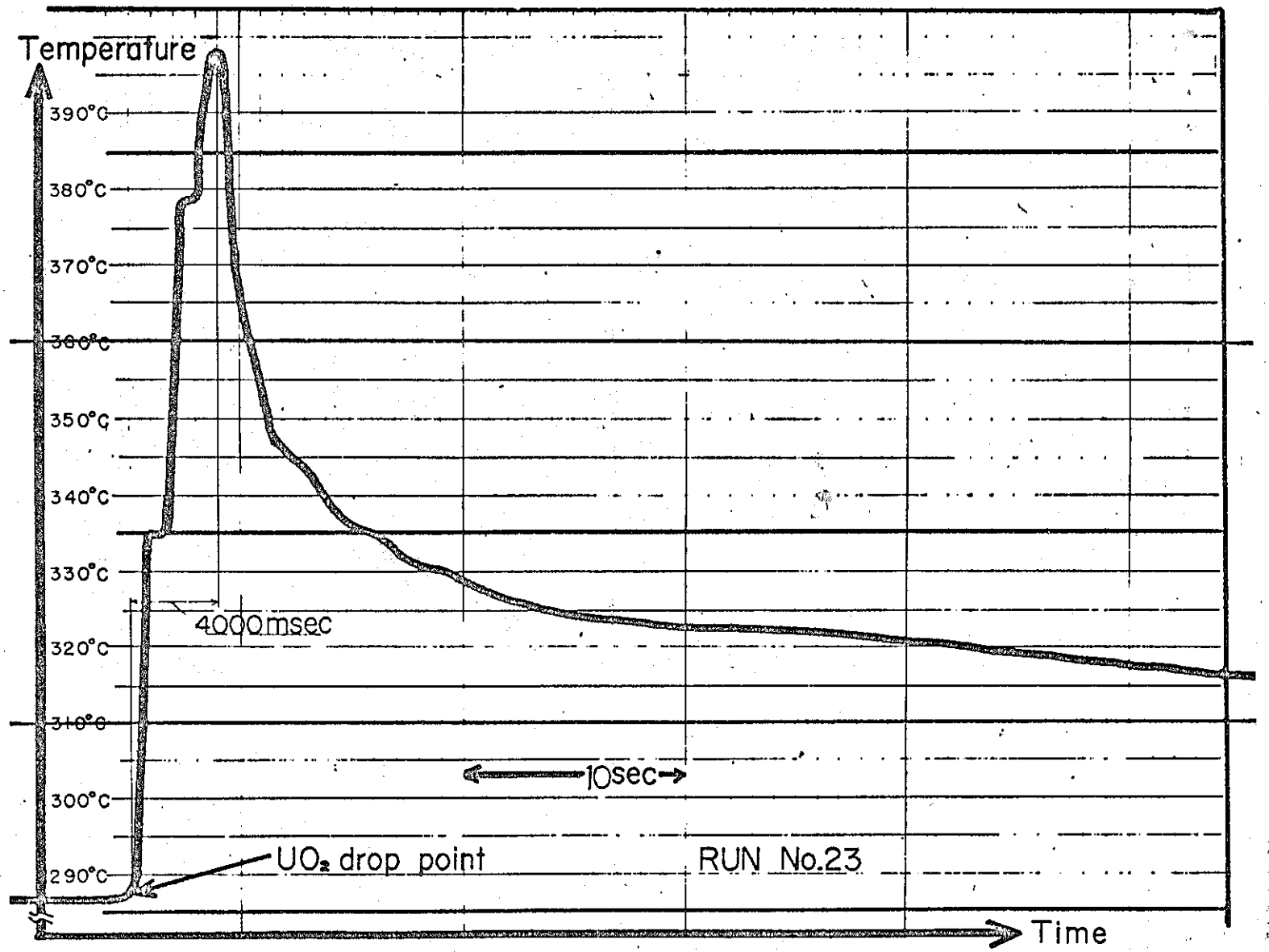

Fig. 8 Sodium temperature distribution.

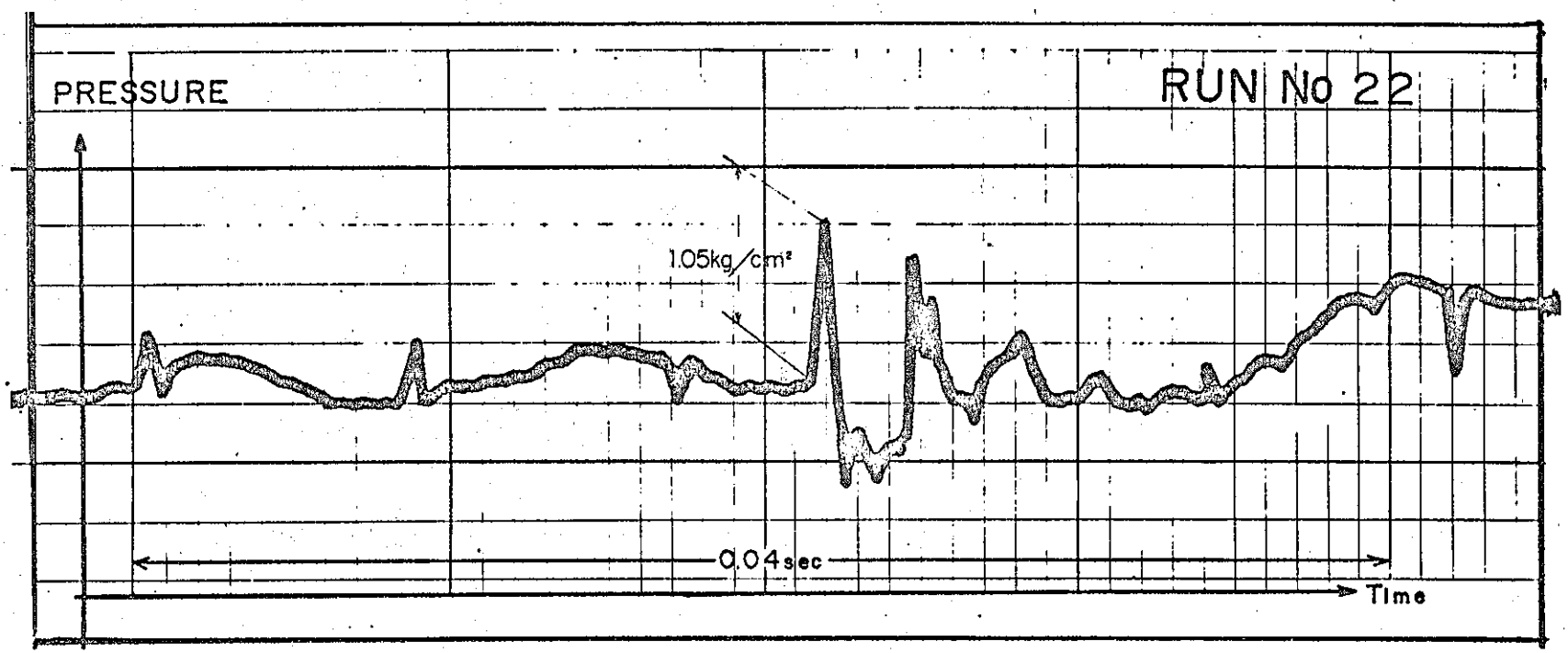

Fig. 9 Typical pressure pulse in the sodium.

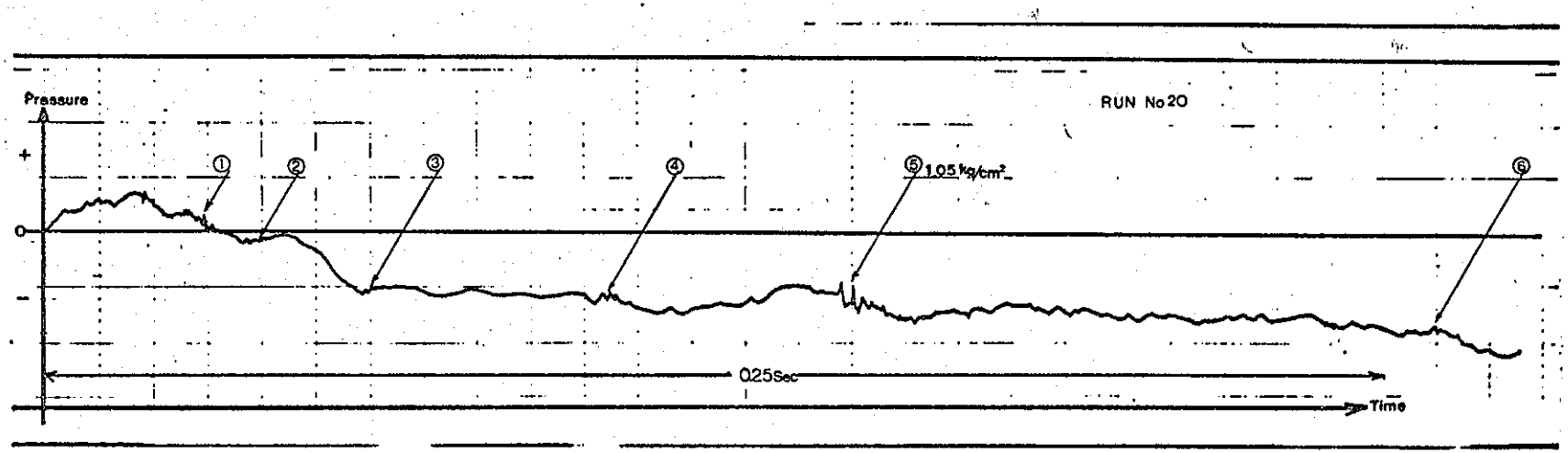

Fig. 10 Pressure hystory for Run 20.

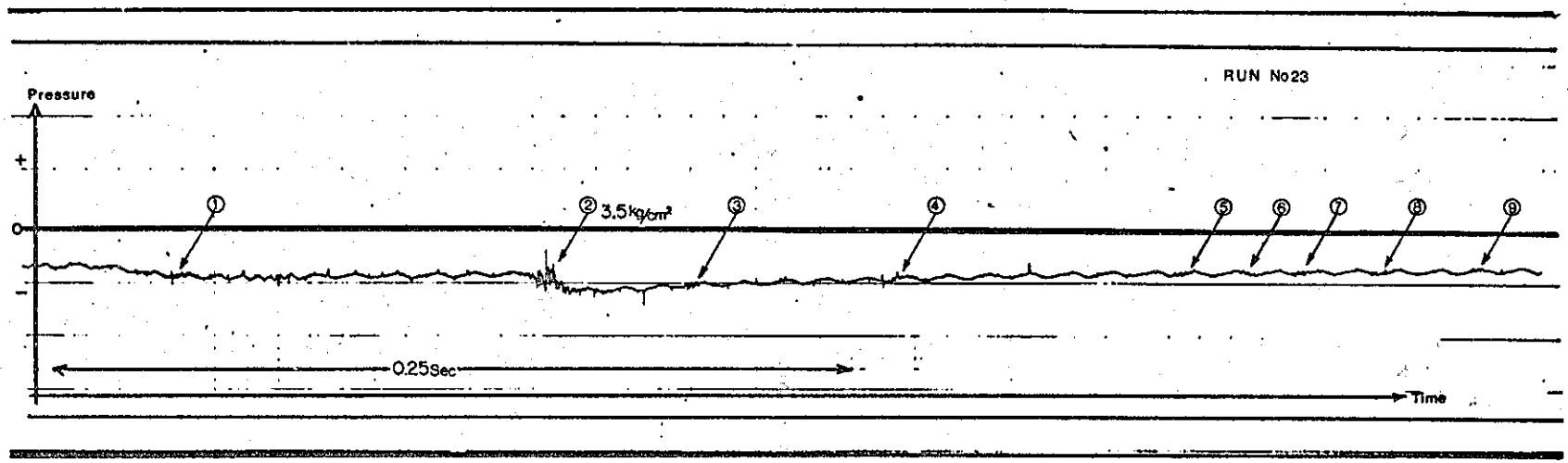

Fig. 11 Pressure hystory for Run 23.

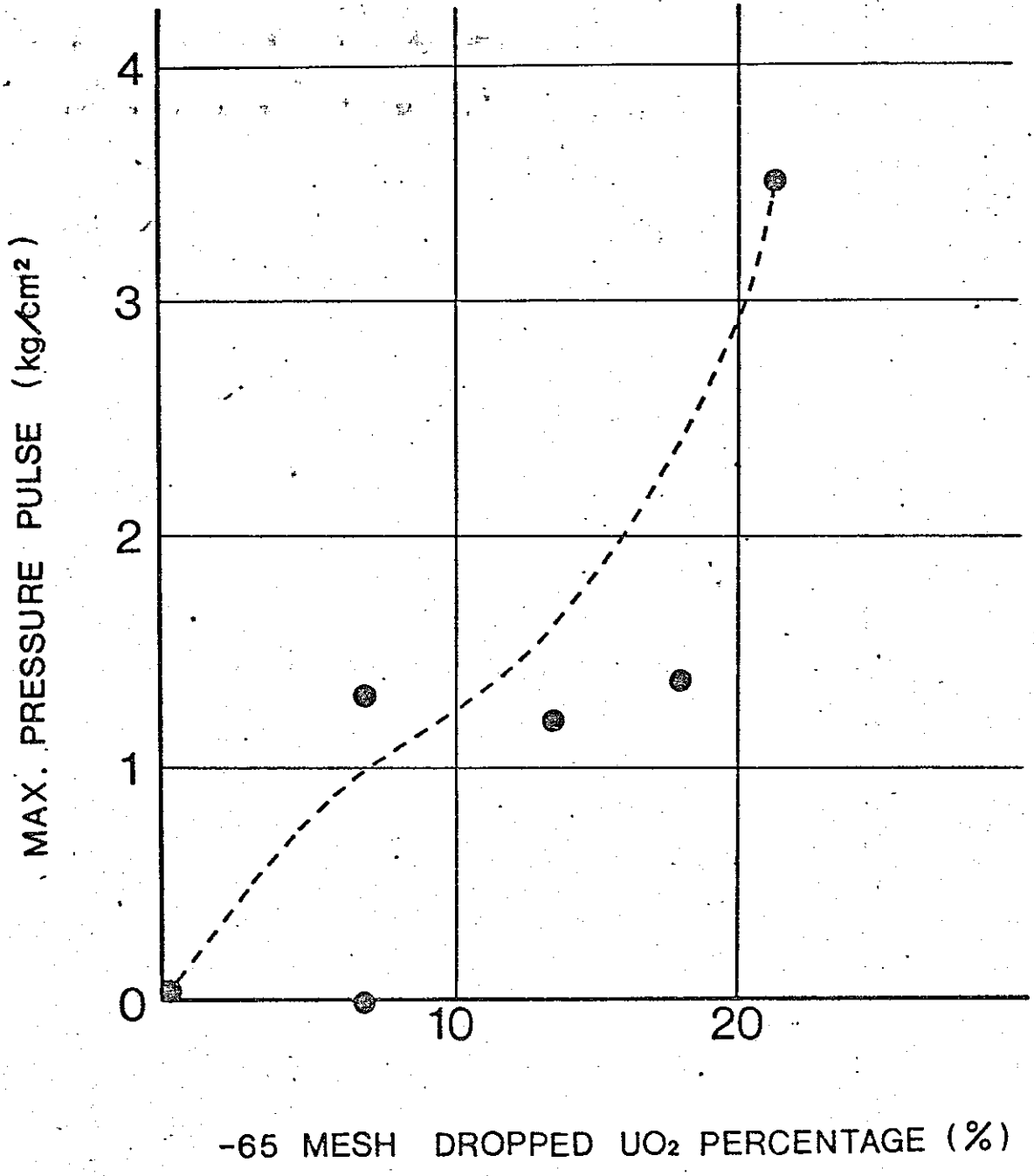

Fig. 12 The correlation between max. pressure peak and UO_2 particle size.

Fig. 13 Collected UO_2 residue of Run 15.

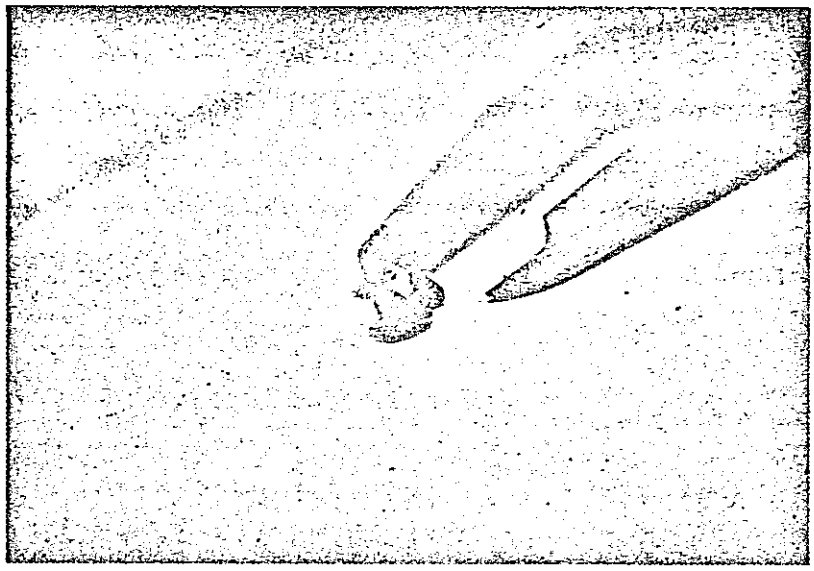

Fig. 14 The sodium in a UO_2 particle.

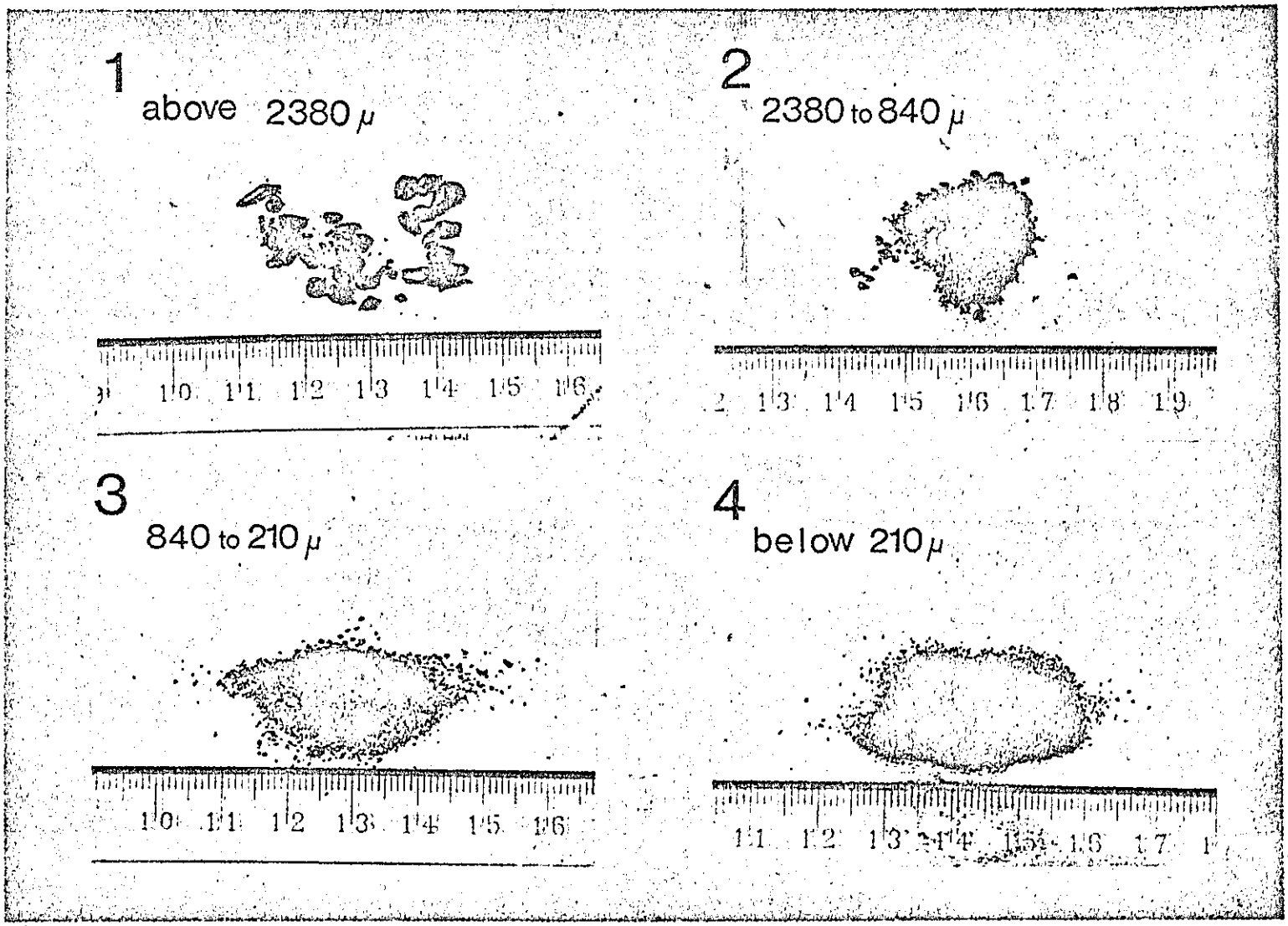

Fig. 15 Separated particles of Run 28.

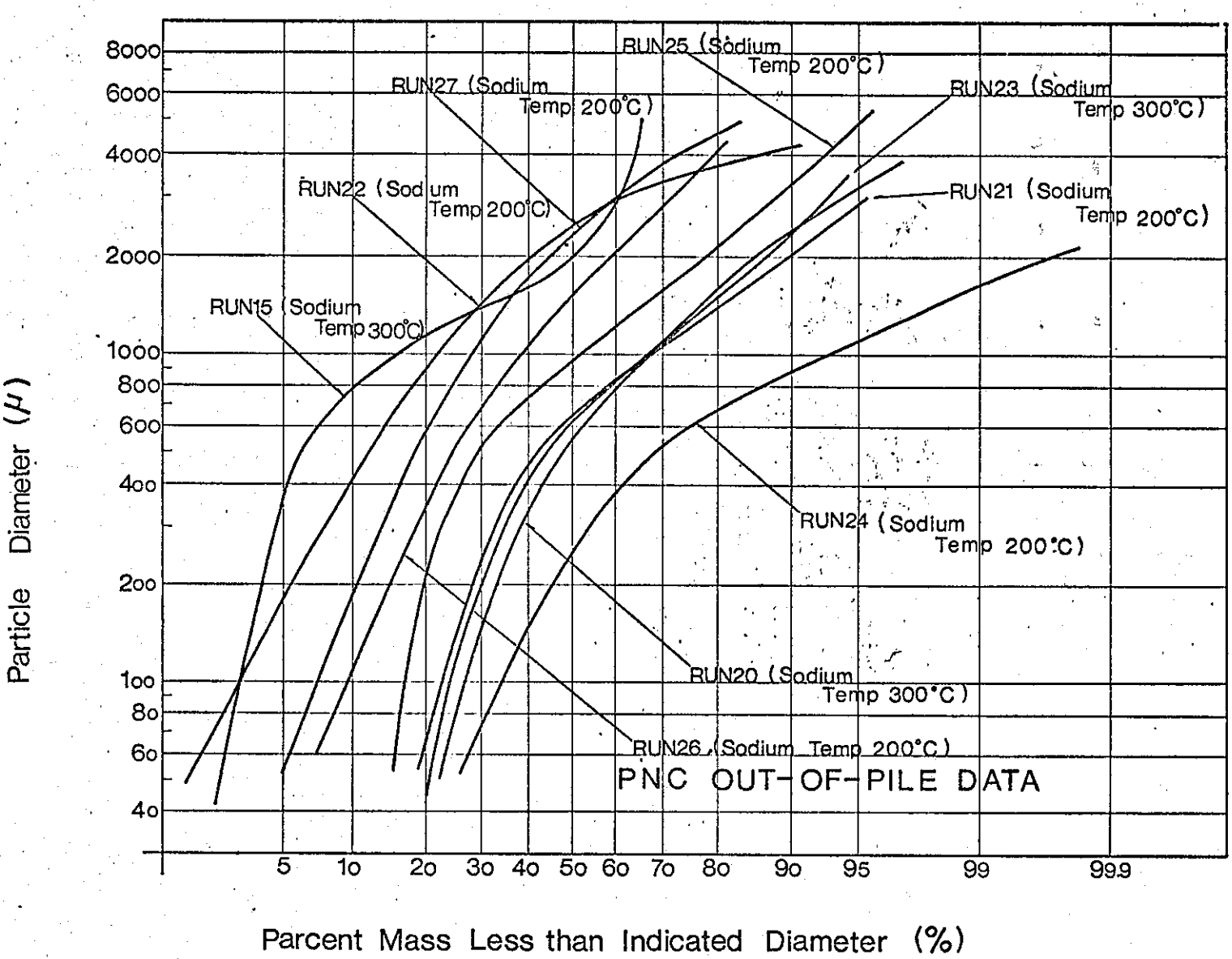

Fig. 16 Particle distributions of UO_2.

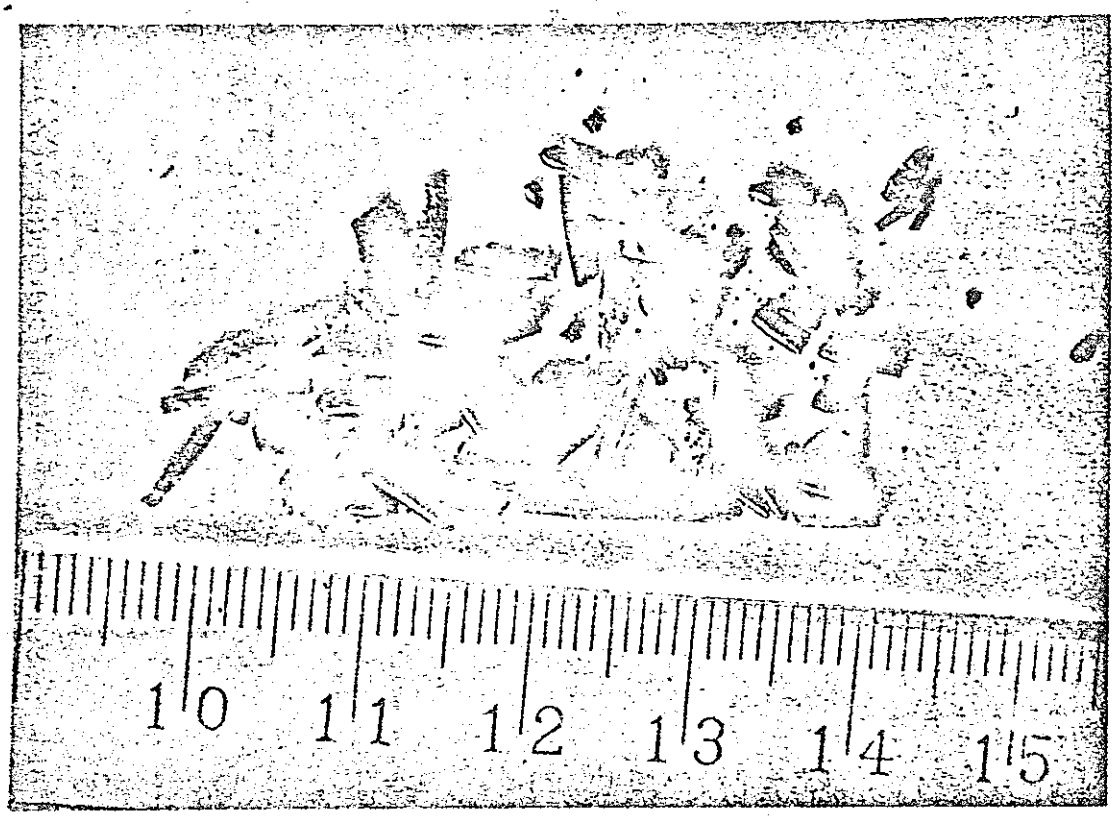

Fig. 17 Large cylindrical particles for Run 25.

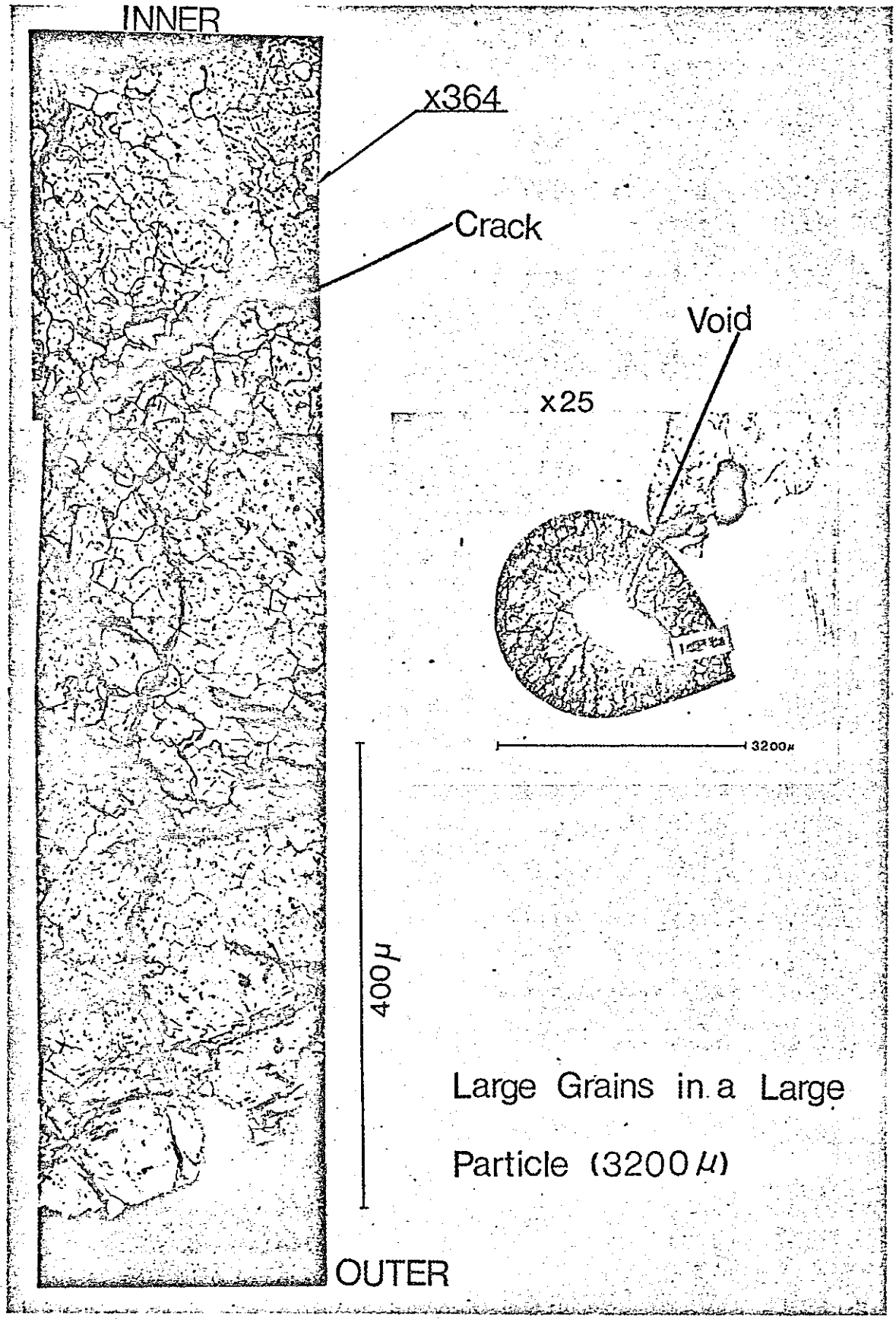

Fig. 18 Large grains in a large particle (3200 μ) for Run 27.

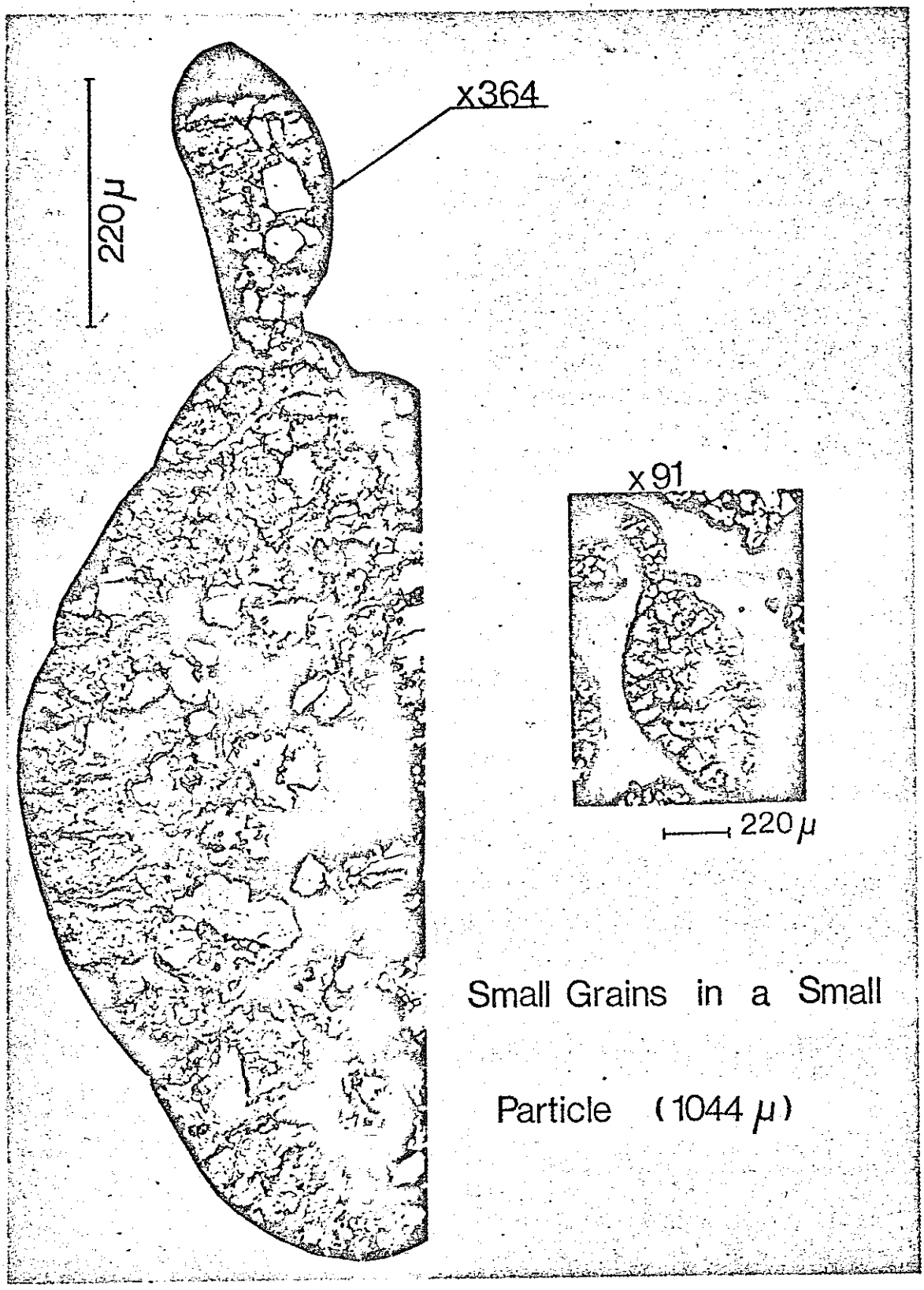

Fig. 19 Small grains in a small particle (1044 μ) for Run 27.

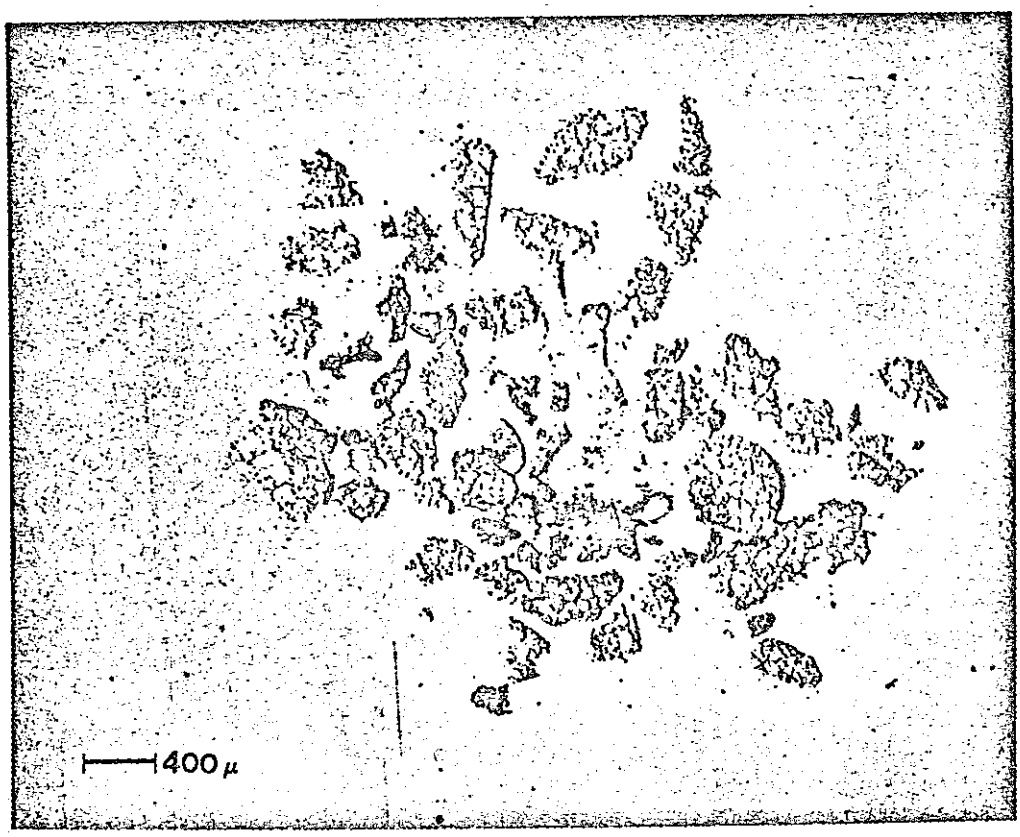

Fig. 20 Small particles for Run 27.

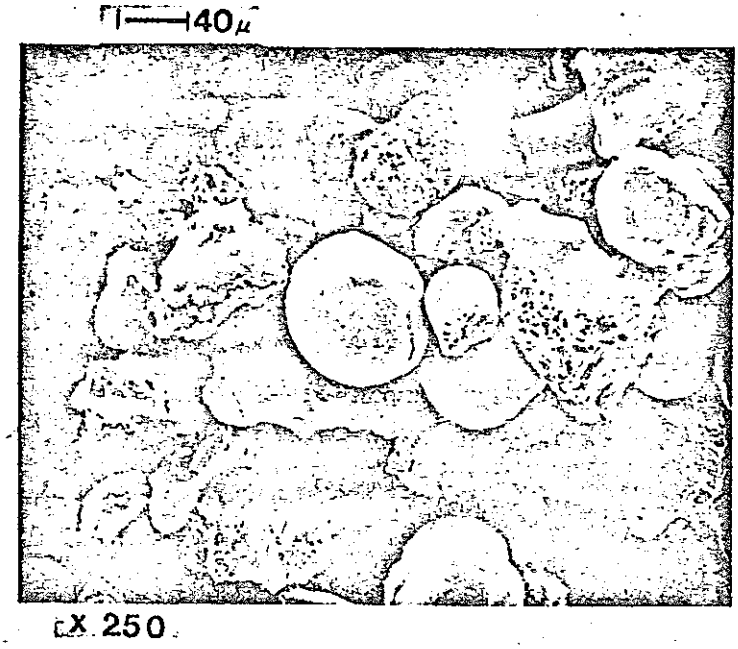

Fig. 21 Small particles (-65 mesh) for Run 23.

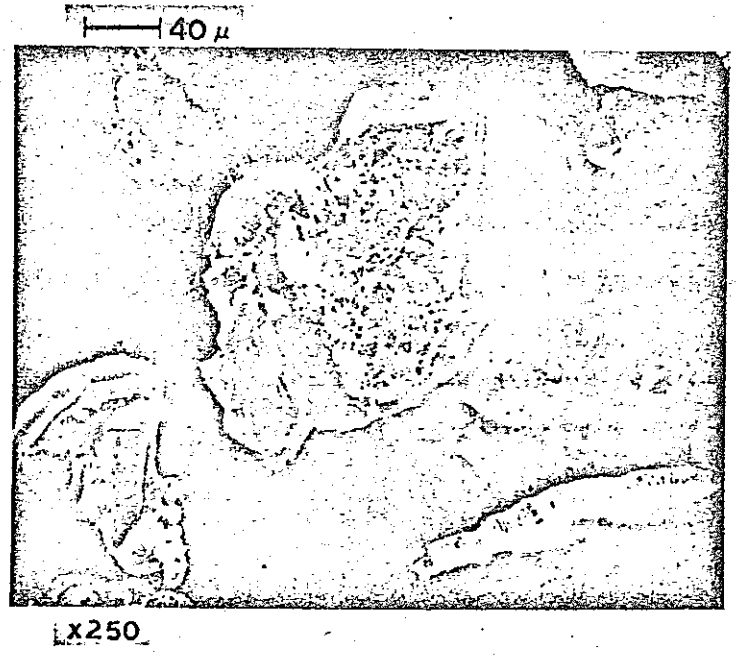

Fig. 22 Small particles (-65 mesh) for Run 20.

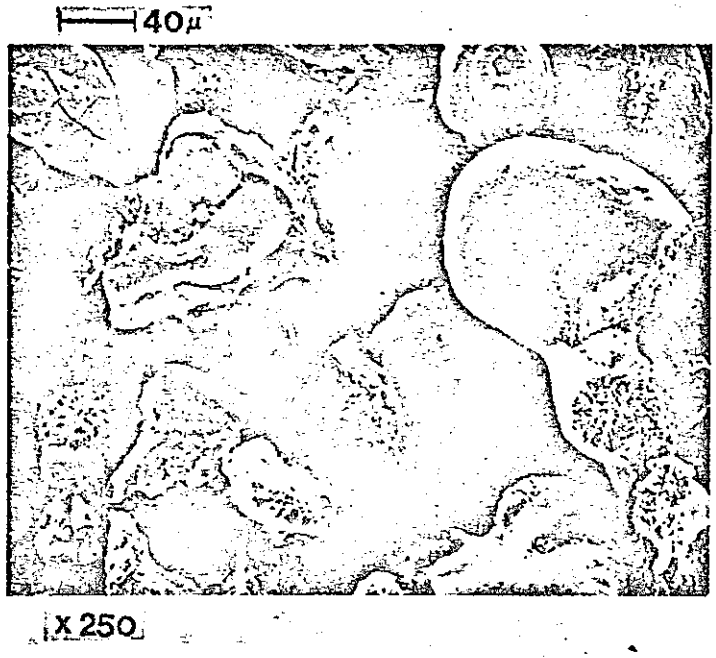

Fig. 24 Close-up of the particle with a hole in Fig. 21.

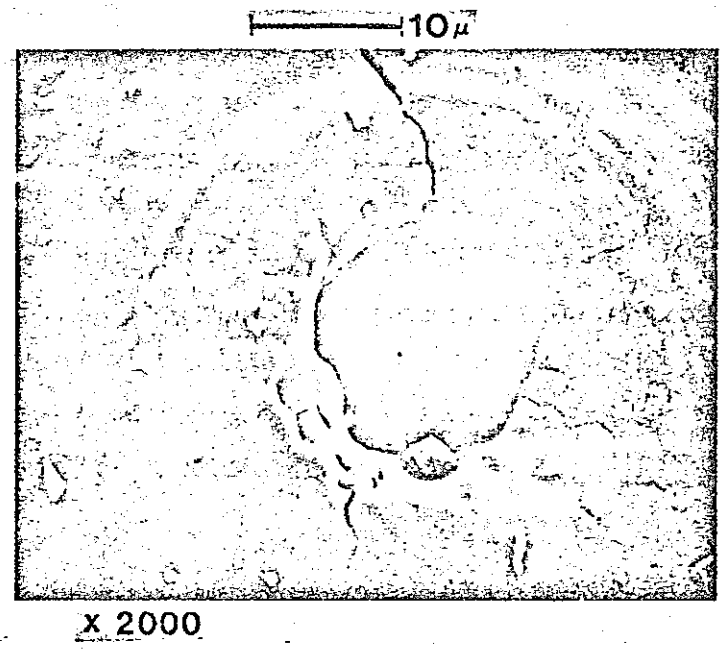

Fig. 23 Small particles (-65 mesh) for Run 22.

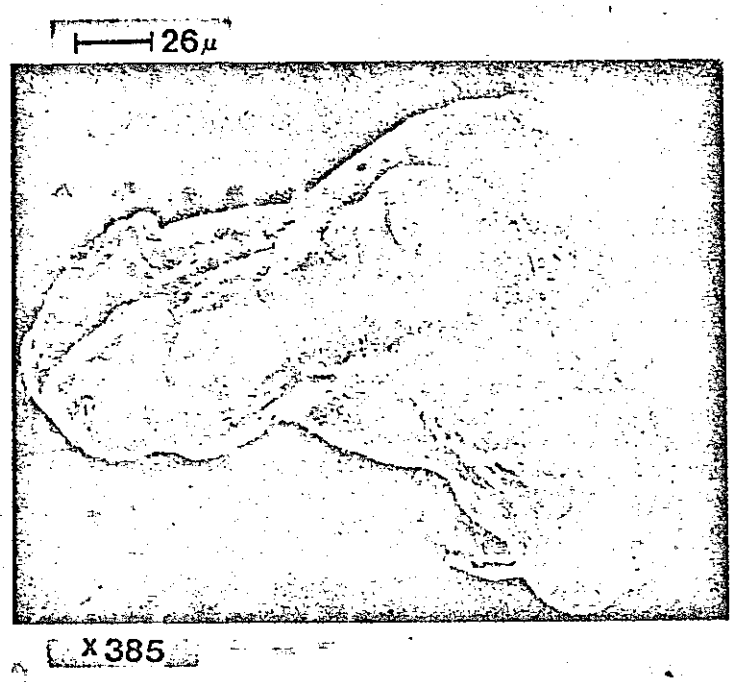

Fig. 25 Typical particle shape (-65 mesh) for Run 20.

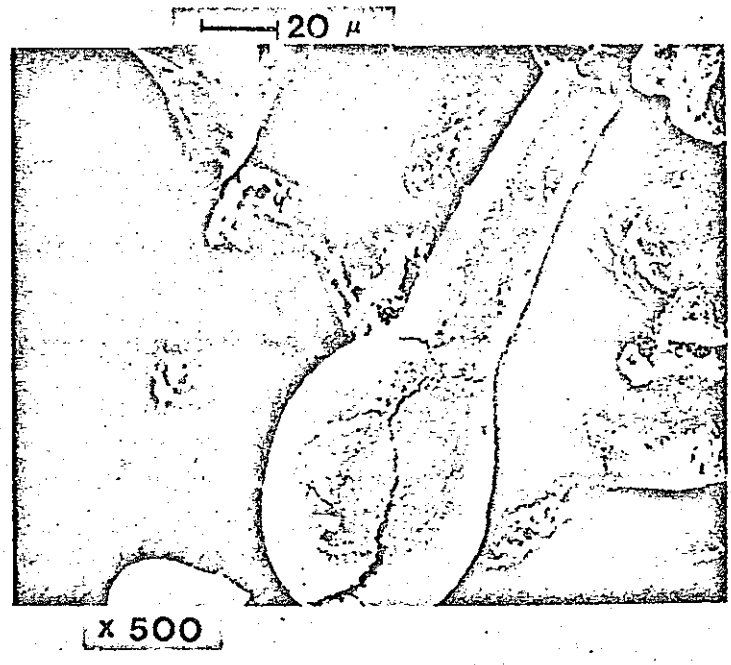

Fig. 26 Liquid droplet shape with large cracks for Run 21.

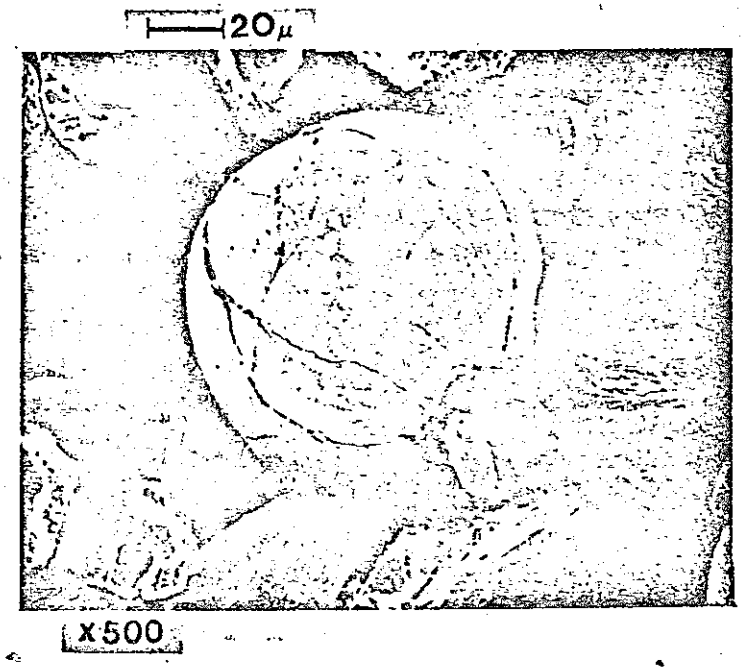

Fig. 27 Spherical shape particle with regular cracks for Run 28.

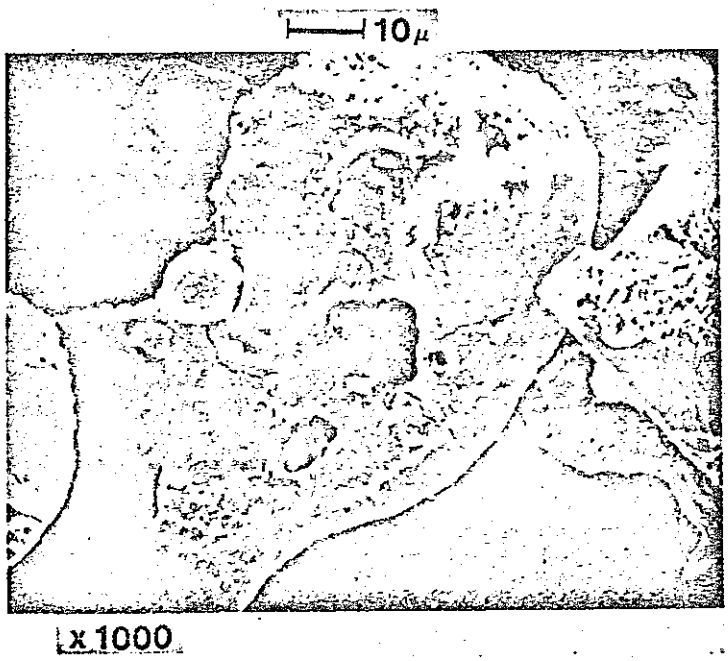

Fig. 28 Two particles fused together for Run 25.

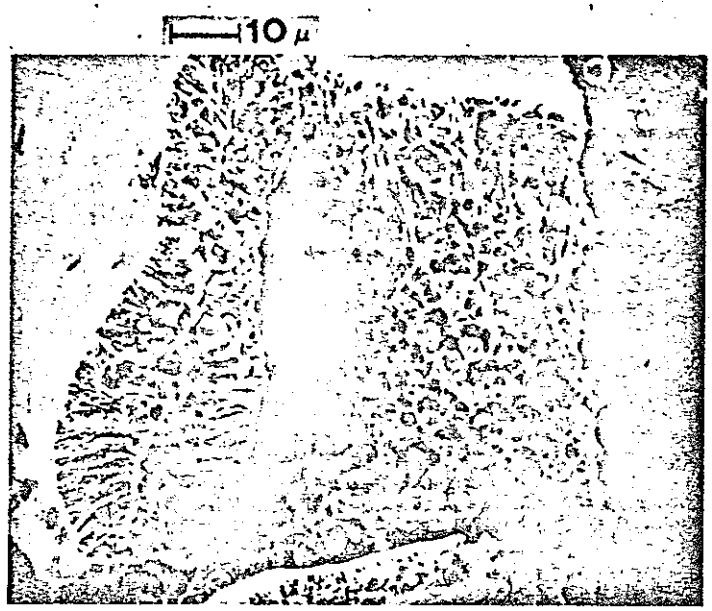

Fig. 29 Columnar grain growth and equi-axial grain growth for Run 25.

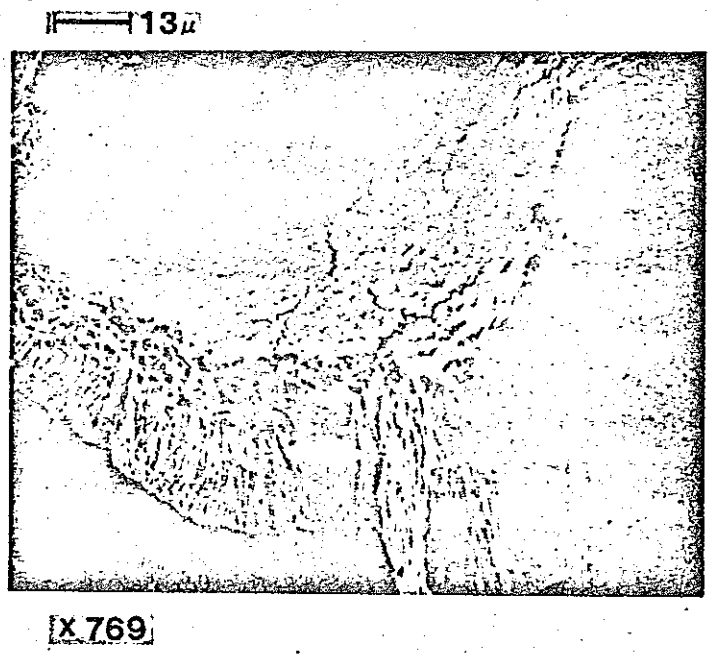

Fig. 30 Equi-axial grain growth at the inside and columnar grain growth to the surface for Run 20.

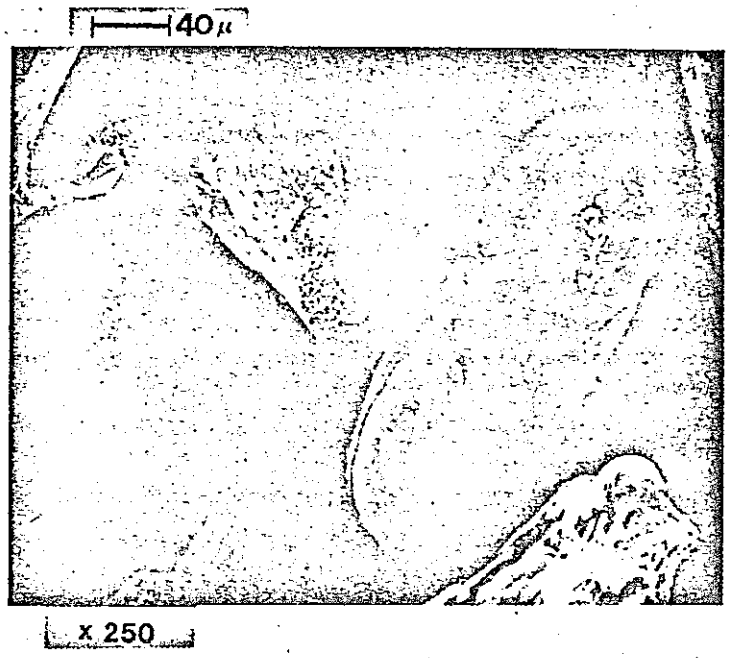

Fig. 31 Typical ellipsoidal particle for Run 20.

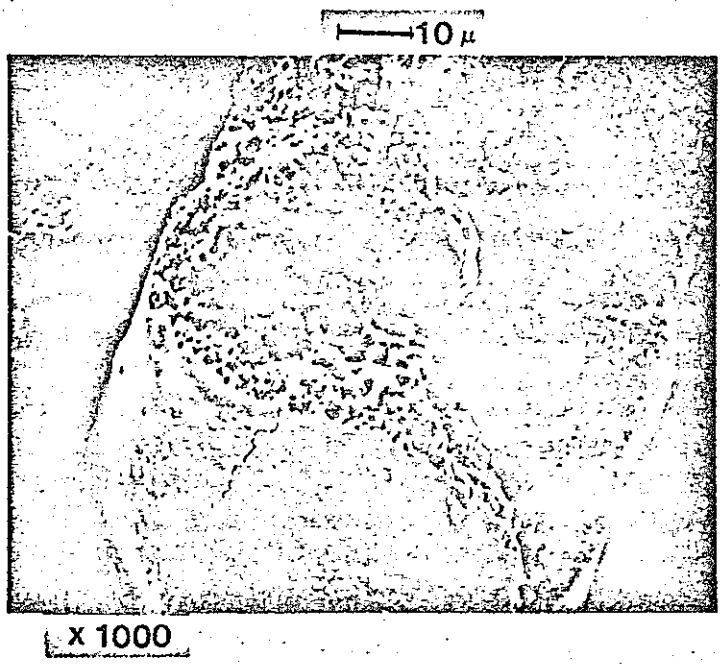

Fig. 32 The quenched type grain for Run 23.

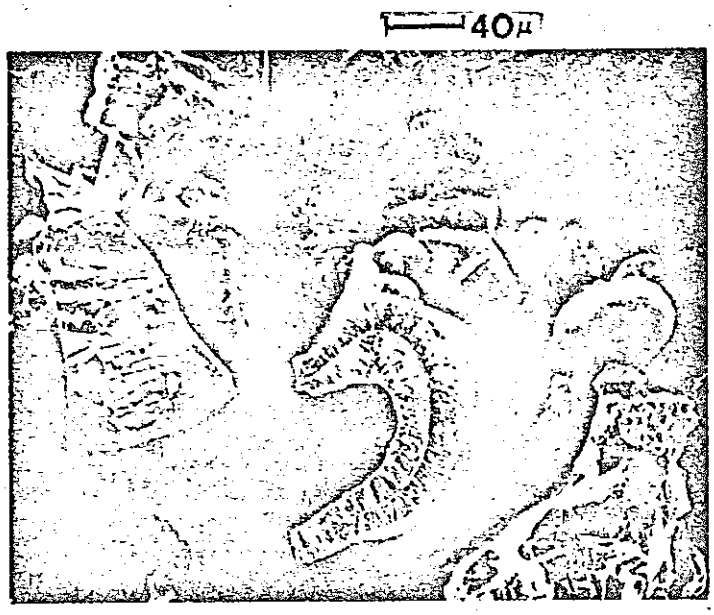

Fig. 33 One solidified particle covered with other particle for Run 21.

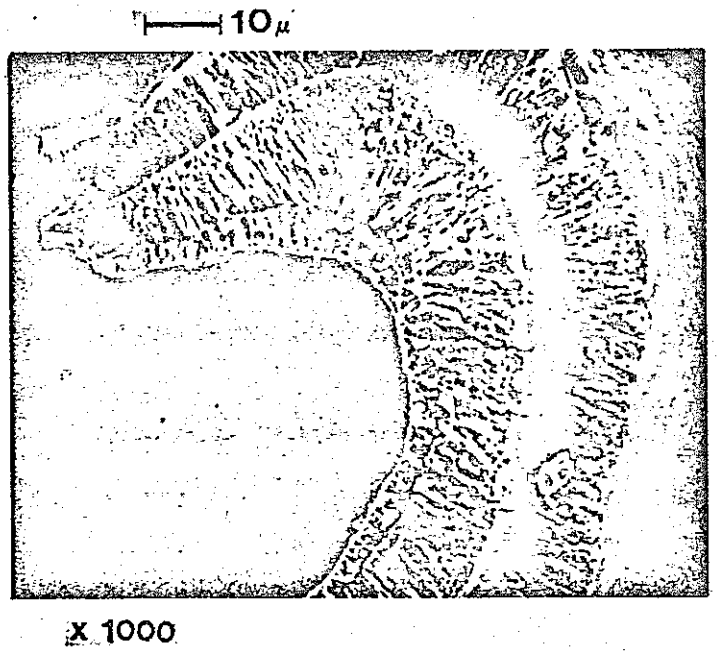

Fig. 34 Close-up of Fig. 33, three different columnar grain growth.

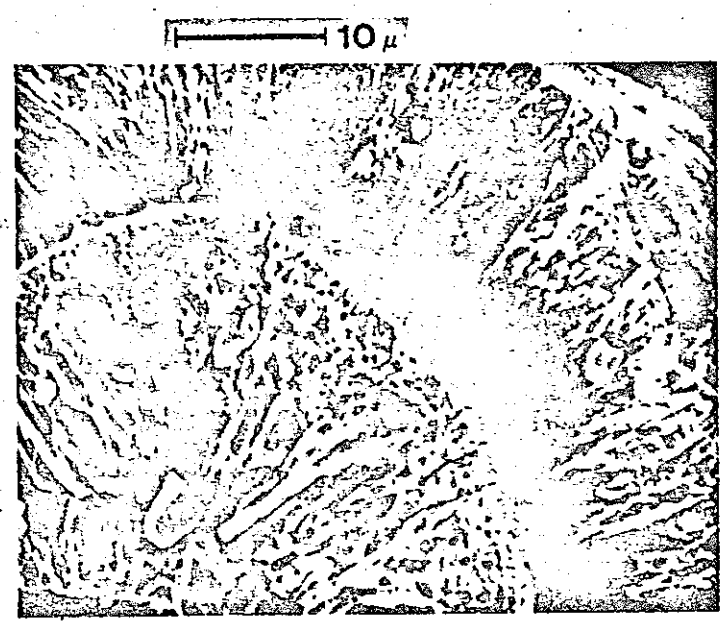

Fig. 35 Close-up of Fig. 34, more different columnar grain growth on the surface.

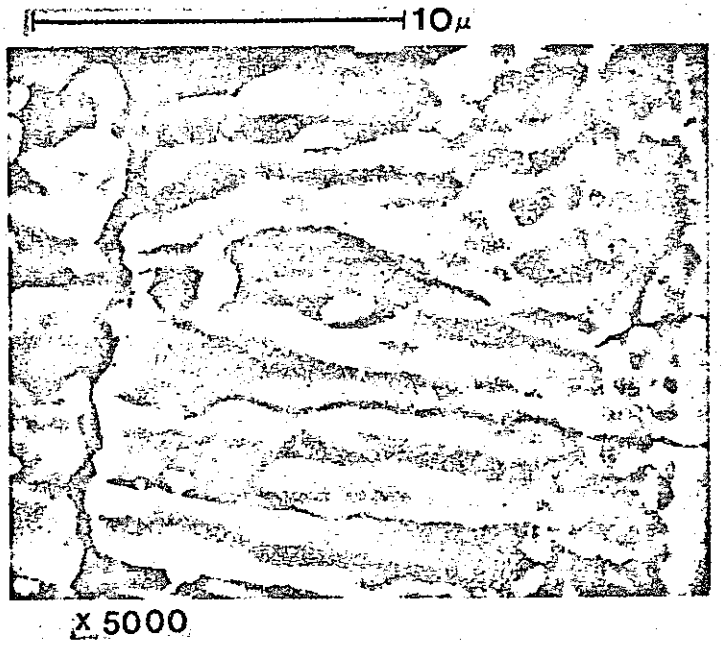

Fig. 36 Close-up of Fig. 35, the surface grain growth.

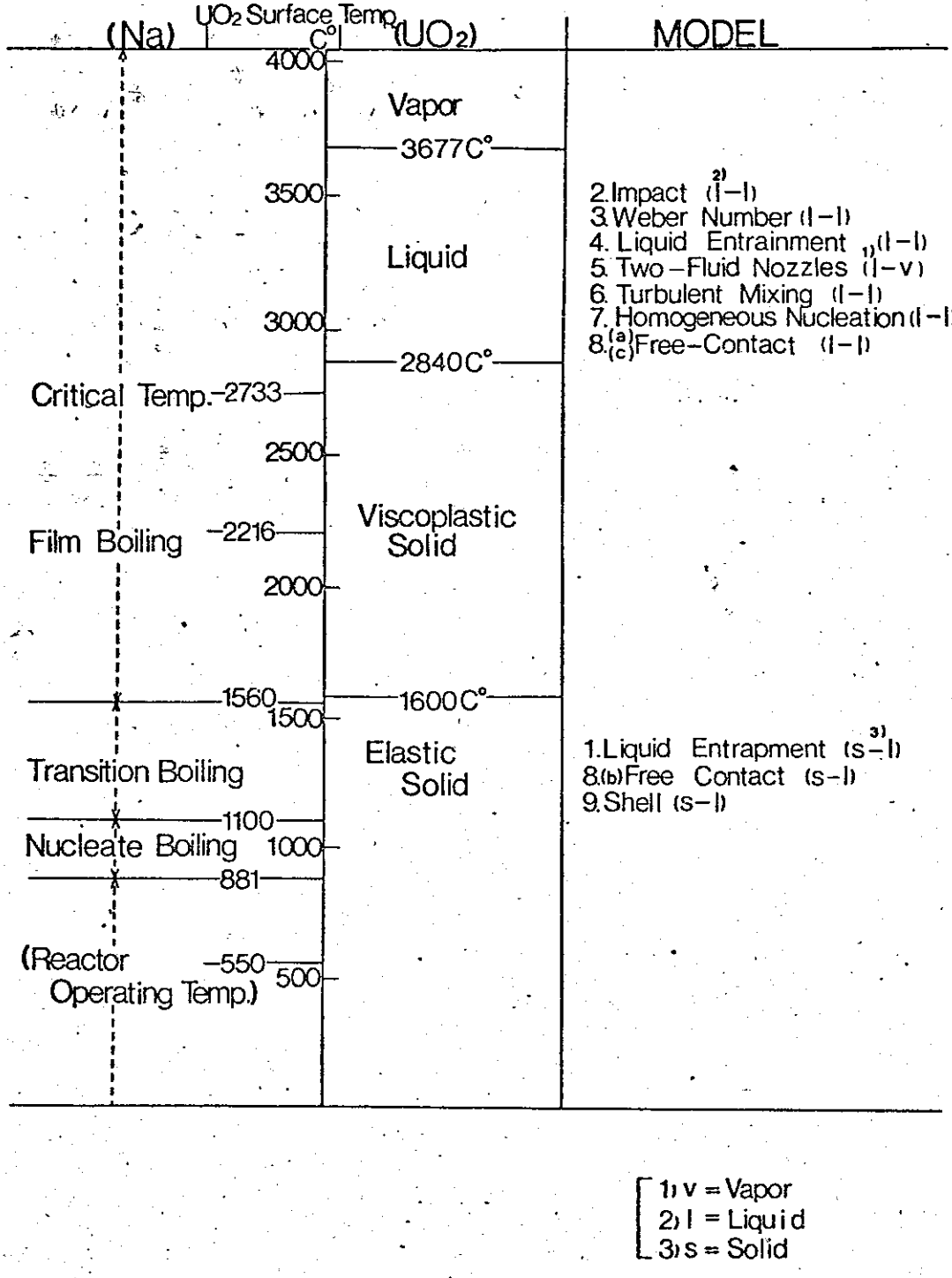

Fig. 37 Schematic Diagram of the Fragmentation Models with the Surface Temperature of the Molten UO_2

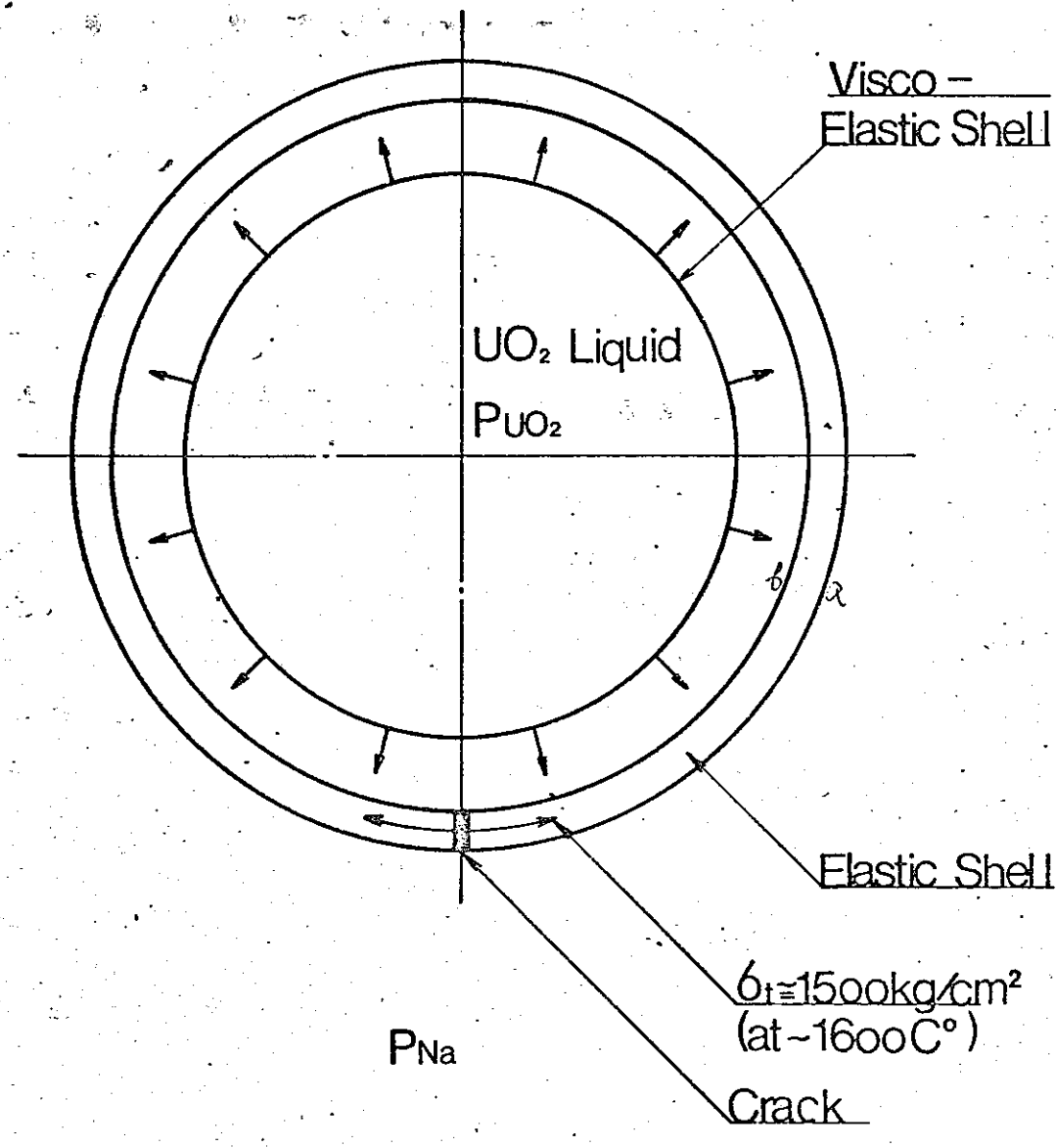

Fig. 38 Concept of the Shell Model

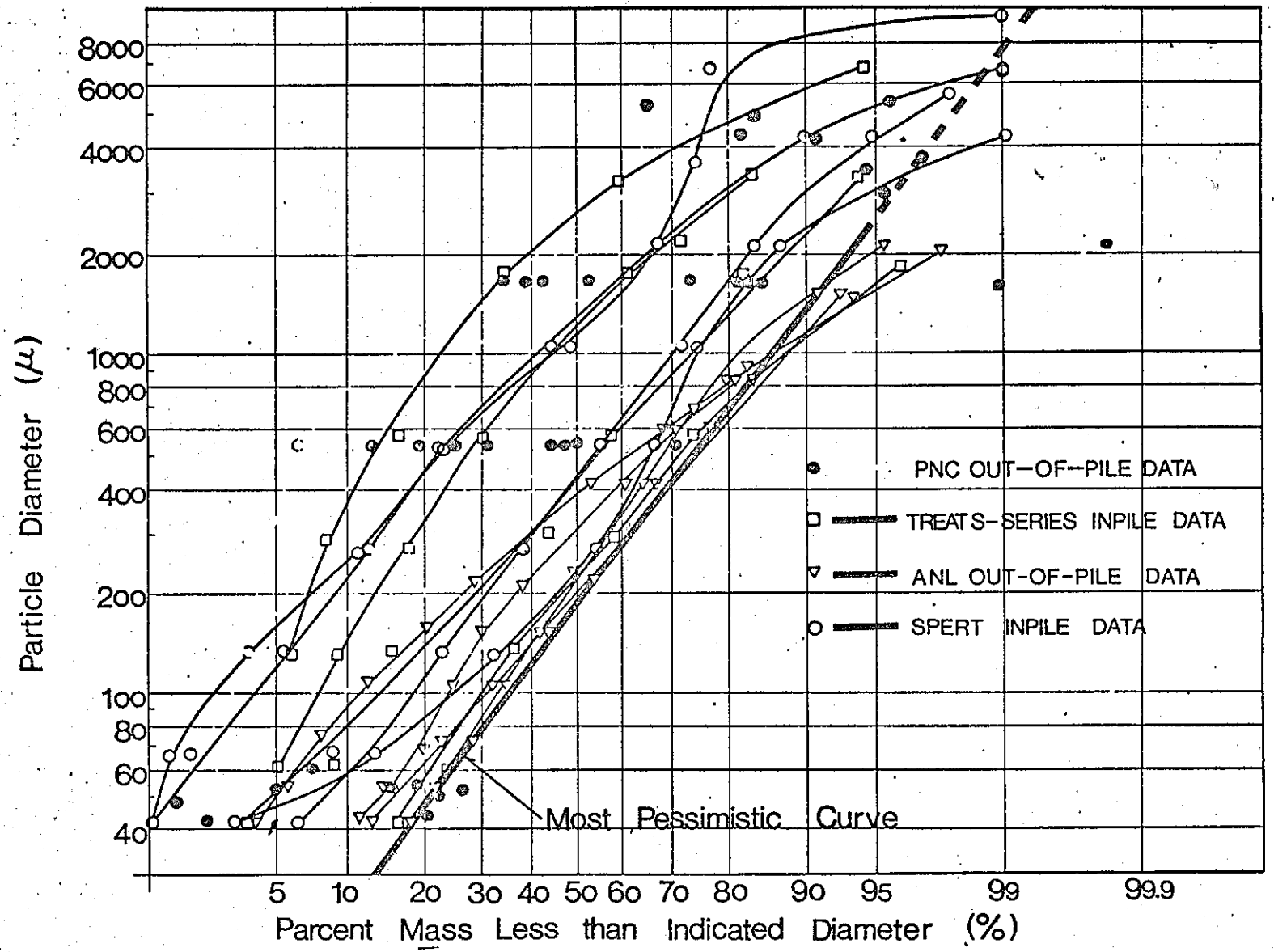

Fig. 39 Fuel particle distributions for the available data.

REFERENCES

1. J. T. A. Roberts and B. J. Wrona, "Deformation and Fracture of UO_2-20 w/o PuO_2," ANC-7945 p.20 June, 1972,
2. G. Long, "Explosion of Molten Aluminum in Water Cause and Prevention," Metal Progress, 71, 107, 1957.
3. S. M. Zivi and R. W. Wright, "Kinetics Studies of Heterogeneous Water Reactors," STL-327-30, 1965.
4. O. Ivins, "Chemical Engineering Division Semi-annual Report," ANL-7399, p. 159, Nov. 1967.
5. F. G. Brauer, N. W. Green and R. B. Mesler, "Metal/Water Explosions," Nucl. Sci. Eng., 31, p.551, 1968.
6. A. Stathhoplos, A. Goldman and J. Herbst, "Coolant Blockage to a Fermi Core-A Central Subassembly at Two Power Levels," NTC-1016-6, July 1969.
7. K. V. Roberts, "Theoretical Calculations on Fuel-Coolant Interactions," CREST Specialist Meeting on Sodium Fuel Interactions, Grenoble, Jan. 1972.
8. H. K. Fauske, "On the Mechanism of Uranium Dioxide-Sodium Explosive Interactions," Nucl. Scien and Eng., 51, 95-101, 1973.
9. D. L. Swift and L. Baker, Jr., "Experimental Studies of the High-temperature Interaction of Fuel and Cladding Materials with Liquid Sodium," ANL-7120, 1965.
10. R. H. Bradley, L. C. Witte and J. E. Cox, "The Vapor Explosion-Heat Transfer and Fragmentation V. Investigation of the Vapor Explosion Phenomenon using a Molten-Metal Jet Injected into Distilled Water," ORO-3936-7, Oct. 1971.

11. M. S. Kazimi et al, "A Criterion for Free-Contact Fragmentation of Hot Molten Materials in Coolants," Trans. ANS, 15, p.835, 1972.

12. K. H. Hsiao et al, "Pressurization of a Solidifying Sphere," J. of Applied Mechanics, p.71, March 1972.

13. M. Amblard et al, "Contact effects Between Molten UO_2 and

14. R. W. Wright et al, "A Delayed Reentry-Type Event in Piston Autoclave Meltdown Test with a Seven-Pin Fuel Bundle," ANS Transaction Vol.14, No.2, p.730, Oct. 1971.

15. D. R. Armstrong, F. J. Testa and D. Raridon, Jr., "Interaction of Sodium with Molten UO_2 and Stainless Steel Using Dropping Mode of Contact," ANL-7890, Dec. 1971.

16. J. A. Mcclure and L. J. Siefken, "Transient Irradiation of 1/4-inch OD Stainless Steel Clad Oxide Fuel Rods to 570 cal/g UO_2," IDO-ITR-100, Oct. 1968.

17. Z. R. Martinson, "Behavior of 5-inch Long, 1/4-inch OD, Zircaloy-2 Oxide Fuel Rods Subjected to High Energy Power Bursts," IN-ITR-107, Aug. 1969.

18. C. S. Olsen, "Measurements of the Reaction of UO_2 with Water for Transient Energy Depositions to 550 cal/g of UO_2," IN-ITR-108, Nov. 1969.